DESIGN AND ANALYSIS OF AN OVERCONSTRAINT WALKING MECHANISM

ÇAĞRI CİNDİOĞLU

SEPTEMBER 2023

ÇANKAYA UNIVERSITY

GRADUATE SCHOOL OF NATURAL AND APPLIED SCIENCES

DEPARTMENT OF MECHANICAL ENGINEERING

M.Sc. Thesis in

MECHANICAL ENGINEERING

DESIGN AND ANALYSIS OF AN OVERCONSTRAINT WALKING MECHANISM

ÇAĞRI CİNDİOĞLU

SEPTEMBER 2023

ABSTRACT

DESIGN AND ANALYSIS OF AN OVERCONSTRAINT WALKING MECHANISM

CİNDİOĞLU, ÇAĞRI
M.Sc. in Mechanical Engineering

Supervisor: Prof. Dr. Sıtkı Kemal İDER
Co-Supervisor: Dr. Özgün SELVİ
September 2023, 74 pages

In this thesis, a walking mechanism is developed from an overconstrained mechanism. The mechanism is composed of eight joints and eight links. The mechanism has one degree of freedom. In this study, the scaling, which is a characteristic feature of the mechanism, is focused on. Due to its scalability, it is shown how the walking path changes by scaling only three of the eight joints. At the beginning of the study, a kinematic analysis and dynamic simulation of the mechanism were performed. In the kinematic analysis, the position equations of the part of the mechanism in contact with the ground, i.e., the end point of the leg, were derived. Since the position equations depend on the parameters, eight different walking paths of the mechanism were obtained. By changing the parameters, the appropriate walking path was determined. Kinematic analysis was performed using Mathematica. In the dynamic simulation section, the walking path generated by the endpoint of the mechanism was obtained. The data obtained from the simulation was compared with the data obtained from the kinematic analysis. Autocad Inventor program was used in the dynamic simulation step. The mechanism parts were designed using Solidworks program. The designed mechanism parts were produced using a 3D printer. A test setup was designed to compare the manufactured mechanism with the data obtained from kinematic analysis and dynamic simulation. The test setup is designed to control

the mechanism under different conditions. Using the video processing method in the test setup, the walking path and velocity graph of the part of the mechanism in contact with the ground were plotted. It was seen that the data obtained from dynamic simulation and kinematic analysis corresponded to each other. Thus, a new mechanism was introduced to the literature.

Keywords: Overconstrained Mechanisms, Mechanism Design, Walking Mechanisms

ÖZET

KISITLI YÜRÜYÜŞ MEKANIZMASI TASARIMI VE ANALİZİ

CİNDİOĞLU, ÇAĞRI
Makine Mühendisliği Yüksek Lisans

Danışman: Prof. Dr. Sıtkı Kemal İDER
Ortak Danışman: Dr. Özgün SELVİ
Eylül 2023, 74 Sayfa

Bu tez çalışmasında, aşırı kısıtlı mekanizmadan, yürüyüş mekanizmasının elde edilmesinden bahsedilmiştir. Mekanizma sekiz eklemden ve sekiz bağlantıdan oluşmaktadır. Tasarlanan mekanizma tek serbestlik derecesine sahiptir. Bu çalışmada, mekanizmanın karakteristik özelliği olan ölçeklendirmeye vurgu yapılmıştır. Ölçeklendirilebilir olmasından kaynaklı, sekiz bağlantıdan sadece üç tanesini ölçeklendirerek, yürüyüş yolunun nasıl değiştiği gösterilmiştir. Çalışmanın başında, mekanizmanın kinematik analizi ve dinamik simülasyonu yapılmıştır. Kinematik analizde, mekanizmanın yere temas eden kısmının, yani ayağın uç noktasının pozisyon denklemleri çıkarılmıştır. Pozisyon denklemleri parametrelere bağlı olduğundan, mekanizmanın sekiz farklı yürüyüş yolu ortaya çıkmıştır. Parametrelerde değişiklik yaparak uygun olan yürüyüş yolunu belirlenmiştir. Kinematik analiz, Mathematica kullanılarak yapılmıştır. Dinamik simülasyon aşamasında, mekanizmanın uç noktasının oluşturduğu yürüyüş yolu elde edildi. Simülasyondan elde edilen veri ile kinematik analizden elde edilen veri karşılaştırılmıştır. Dinamik simülasyon aşamasında Autocad Inventor programı kullanılmıştır. Mekanizma parçalarının tasarımı Solidworks programı kullanılarak yapılmıştır. Tasarlanan mekanizma parçaları 3D yazıcı kullanılarak üretilmiştir. Üretilen mekanizmanın, kinematik analizden ve dinamik simülasyondan elde edilen verilerle karşılaştırılması için test düzeneği tasarlanmıştır. Test düzeneği mekanizmayı farklı koşullarda test edebilecek

şekilde tasarlanmış ve üretilmiştir. Oluşturulan test düzeneğinde görüntü işleme metodu kullanılarak mekanizmanın yere temas eden kısmının yürüyüş yolu ve hız grafiği çıkarılmıştır. Dinamik simülasyon ve kinematik analizden elde edilen verilerle, bu verinin birbirlerini karşıladığı görülmüştür. Böylece literatüre yeni bir mekanizma kazandırılmıştır.

Anahtar Kelimeler: Yürüyüş Mekanizmaları, Mekanizma Tasarımı, Aşırı Kısıtlı Mekanizmalar

ACKNOWLEDGEMENT

I would like to thank my wife, DZHANETTA CİNDİOĞLU, who supported me not only during my master's degree but also in every moment of my life, sacrificed her social life for me, took on many responsibilities and lightened my burden, and made it easier for me to complete my life and my master's degree.

I would also like to thank my esteemed teacher Dr. ÖZGÜN SELVİ, who was more like a brother than a teacher-student relationship, who responded to my questions even late at night, who worked tirelessly with me, who changed my perspective on life and enlightened me with his knowledge, and my esteemed teacher Prof. Dr. SITKI KEMAL İDER, who enlightened me with his knowledge both during the undergraduate and master's degree, and who did not withhold his support during the thesis period.

I would especially like to thank my family, who have never lost their trust in me and whose support I have always felt. If I have achieved anything, it is thanks to you.

I would also like to thank CİHAN IRGI, FAZLI BURAK KURT and KEMAL KONYALI for the ideas and support they gave me.

TABLE OF CONTENTS

LIST OF TABLES

LIST OF FIGURES

LIST OF SYMBOLS AND ABBREVIATIONS

cm	: Centimeter
mm	: Millimeter
s	: Second
M1	: Motor 1
M2	: Motor 2
a	: Acceleration
V	: Velocity
CW	: Clockwise
CCW	: Counterclockwise
CAD	: Computer Aided Design
fps	: Frame per second
DoF	: Degrees of Freedom

CHAPTER I

INTRODUCTION

Walking mechanisms offer several advantages over conventional modes of locomotion such as wheels or tracks. These advantages include reduced vibration through the discrete contact of endpoints, the ability to traverse multiple terrains with minimal contact area, controllable vehicle height, increased traction, climbing abilities, and obstacle negotiation. Inspired by the walking motion of humans, insects, and animals, walking mechanisms have been developed and used in various applications such as rehabilitation, search and rescue, military, and entertainment. As such, they have gained significant attention in the field of robotics, where they offer a versatile and adaptable means of locomotion.

Several researchers create, analyze, and interpret new mechanisms. One of the popular walking mechanisms due to its organic motion is presented in Jansen's work [1]. Amanda Ghassaei [2] has designed and analyzed the Crank-Based Leg Mechanism. In her study, she took Theo Jansen's [1] mechanism as a reference. In her research, she compared the walking paths required for walking. As a result of the optimizations made, the aimed mechanism was designed and produced. Kim et al. [3] referenced Theo Jansen's [1] mechanism in their study. In the designed mechanism, the target walking path is determined, and then the desired path is obtained by using the firefly algorithm. Nansai et al. [4] analyzed the dynamics of a four-legged Theo Jansen mechanism robot. They used the projection method while making an analysis. In the future, they aimed to develop this subject and to use it in different areas in real life. Kim et al. [5] designed a Klann Mechanism [29] that can travel both in water and on land. In the design of the mechanism, the maximum height that it can travel in water was calculated. As a result of the optimizations, they achieved an economic saving of 62% compared to the first model. Ottaviano et al. [6] designed and analyzed a single-degree-of-freedom rickshaw mechanism. In order to test the accuracy of the mechanism, a test setup was created and tested under various conditions. Furthermore,

Deb and Tiwari [7] solved the optimization problem simultaneously using evolutionary multi-objective optimization for the exact mechanism. Selvi et al. [8] used the firefly algorithm to optimize a planar linkage for the minimum number of links for walking. Selvi et al. [9] designed an overconstrained walking mechanism with a single degree of freedom. They selected how the designed mechanism would form a path during walking. They performed optimizations on the links of the mechanism to obtain the selected path. They used the firefly algorithm in the optimization. Geona et al. [10] designed and simulated a walking mechanism with a single degree of freedom similar to human walking. They aimed to produce the designed nine-bar mechanism in the following stages and to carry out experiments. Batayneh et al. [11] designed an eight-bar walking mechanism with a single degree of freedom similar to the human gait. During their design, the main emphasis was on the slenderness of the leg and the shape of the walking path. They stated in their study that although it was not manufactured, it was designed to be suitable for production. Desai et al. [12] presented a planar Peaucellier-Lipkin type with eight walking mechanism links and optimized the dimensions for a straight line using genetic algorithms. Fedorov et al. [13] designed a walking mechanism with a single degree of freedom. The defining feature of their mechanism is that when it faces an obstacle, the walking path changes according to this obstacle. It was aimed that such a mechanism would exhibit a highly efficient gait under off-road conditions. Wu and Yao [14] developed and tested a walking leg that can transform its topological structure by shifting the joint type. Tsai et al. [15] designed a single-degree-of-freedom mechanism. They aimed to perform walking in various land conditions with their design. They also showed improvements in the actuation torque by optimizing the link dimensions. Kamidi et al. [16] designed a six-link mechanism with a single degree of freedom. Four of the designed mechanisms were positioned on a platform to create a fast-walking robot. In the next stage, they aimed to optimize the foot trajectory. Gong et al. [17] designed a four-legged climbing robot with two degrees of freedom and handling capability. James et al. [18] designed a single-degree-of-freedom bi-pedal walking robot. The robot was manufactured and tested. In the tests, they mentioned that it was more inefficient at low speeds than at high speeds and that mentioned about it should improve. They used the Klann [29] mechanism as a reference for walking and gripping. They fabricated the designed mechanism and performed experiments. Bhavsar et al. [19] have performed kinematic and dynamic analyses of the eight-legged Theo Jansen mechanism. In addition to these

analyses, they have shown the changes in energy consumption as a result of the changes made. Li et al. [20] analysed the walking of dogs and derived a walking path. They designed a walking mechanism with reference to this path. Wang et al. [21] designed a mechanism with reference to the joints of kangaroos and performed kinematic analyses of the designed mechanism. Gonzalez et al. [22] designed a legged or hybrid robot with 3 degrees of freedom. The designed robot has lateral sliding, straight-line drawing, and obstacle-jumping capabilities. This robot was designed and successfully passed the tests. Daniel et al. [23] designed a new walking mechanism with reference to Theo Jansen's mechanism [1]. In their design, they aimed to optimize the step length and energy consumption of the Theo Jansen mechanism. The mechanism has been produced and they have achieved the aimed goal. Sven Böttcher [24] talked about legged and wheeled locomotion in his seminar. In the walking mechanisms chapter, he talked about the foot configurations required for single, double, four and six-legged mechanisms to be able to walk. He explained the position of the legs with respect to the centre of gravity of the robot. Zhonghua et al. [25] designed an eight-link mechanism with a single degree of freedom. Using four of the mechanisms, they designed a robot to climb stairs. Anthony et al. [26] designed a Klann [29] mechanism with two degrees of freedom controlled by two motors and capable of traveling both on land and in water. They have completed position and velocity analyses. As a result of the analyses, the mechanism was manufactured and tested. As a result of their studies, they have shown that the mechanism works successfully. Al-Shammari et al. [27] designed a hexapod robot for use in different land conditions. Firstly, they analysed the analyses for a single leg and then analysed according to the operation of 6 legs together. As a result of the successful analysis, the mechanism was produced and successfully executed. Yuping Gu et al. [28] built a 4-legged robot with an overconstrained link with a single degree of freedom. This robot is characterized by being omnidirectional and its rotation diameter is 0.2 times its height. The robot is capable of forward, lateral, and vertical movements. As a result of the kinematic analysis of the mechanism, the mechanism was produced and tested. The tests showed that the mechanism was successful. They mentioned that they are planning an algorithm to affect the design process in future work. Batayneh et al. [29] designed a walking mechanism representing human gait with a single degree of freedom. J.C. Klann [30] designed a single degree of freedom mechanism to represent animal gait. He patented this mechanism in 2001. This mechanism has been a reference

for many people studying in the literature. Optimization [5] and improvement [17] of the Klann mechanism are studied. Hao et al. [31] designed a walking mechanism with a single degree of freedom. They aimed to make the mechanism simpler than other mechanisms but to serve the same purpose. They created a walking robot by using four of the mechanism together. The analyses showed that the mechanism was successful. Xianwen Kong [32] has analyzed the kinematics of a 6-joint single loop overconstrained spatial mechanism. He reduced the kinematic analysis of the mechanism to the solution of a second-order equation in a single variable. He also analyzed the free-state motion of the mechanism. Lu et al. [34] designed a 4-legged robot with 2 degrees of freedom. In their study, they analyzed the kinematic analysis and walking path of the robot. They tested the working of the mechanism with an experiment. Lu et al. [34] designed a hybrid robot with wheels and legs. These legs are activated in case the robot climbs stairs or jumps obstacles. Considering this situation, they analyzed the gait of the foot mechanism. They tested a prototype of the robot in various conditions and proved that it was successful. Saha [35] built a sweeping robot using Hoeken and Pantograph mechanisms. He has produced and successfully operated the robot. The sweeping motion represents a walking path. By revising this mechanism, a walking mechanism can be obtained. Chen et al. [36] designed an 8-bar walking mechanism. They highlighted that the eight-bar walking mechanism is superior to the four-link and six-link mechanisms and can better meet the required movement needs. They optimized the method they used in the design of the mechanism with computer-aided programs.

In the second chapter of this thesis, a spatial two-loop single DoF overconstrained ($\lambda=5$) walking mechanism is suggested for a walking mechanism. Kinematic analysis and dynamic simulation of the mechanism are performed. Position equations are derived from the kinematic analysis. Different alternative results of the mechanism are derived from the position equations. stride to height of the step ratio and stride to leg height ratio were taken into account and the best one was selected from the alternative results. Dynamic simulation was performed according to the selected mechanism.

In the third chapter, a test setup was established to verify the correctness of the data obtained from the analysis and simulation. In the test, the velocity values of point P from the dynamic simulation and the walking path were obtained.

In the fourth chapter, dynamic simulation and test results are discussed. In the dynamic simulation, comparisons of the proposed overconstrained mechanism at different scales and comparisons of Theo Jansen, Ghassaei, Fourbar Pantograph, Desai, Klann, and proposed overconstrained mechanisms with the same height were made. The walking path and velocity graphs obtained from the test results are compared.

In the fifth chapter, the number of links and joints, scalability, speed comparison of the P point, the ratio of the mechanism's length to the straight line, the ratio of the fluctuations in the straight line to the height of the walking path and the ratio of the area covered by the mechanism to the straight line are compared.

In the conclusion, it is highlighted that the mechanism is verify. A new mechanism for those who will work in this study area has entered the literature. Future works for the development of the mechanism are highlighted.

CHAPTER II

OVERCONSTRAINED LEG MECHANISM

Before starting the design of the overconstrained walking mechanism, the work of Selvi et al. [9] on this subject was studied. In this study, a scalable walking mechanism with single degree of freedom is shown in Figure 1 [9]. The design was continued by taking this mechanism as a reference.

When the study was analyzed, it was seen that there were some weaknesses. Considering the walking mechanism of this mechanism, the most important part is that it draws straight at the point where it touches the ground. But in the study, the straight line was not smooth enough. For this purpose, we aimed to make a new design. While designing the new mechanism, an additional spherical loop was added to the reference mechanism. By doing this, we aimed to obtain more results by increasing the number of parameters.

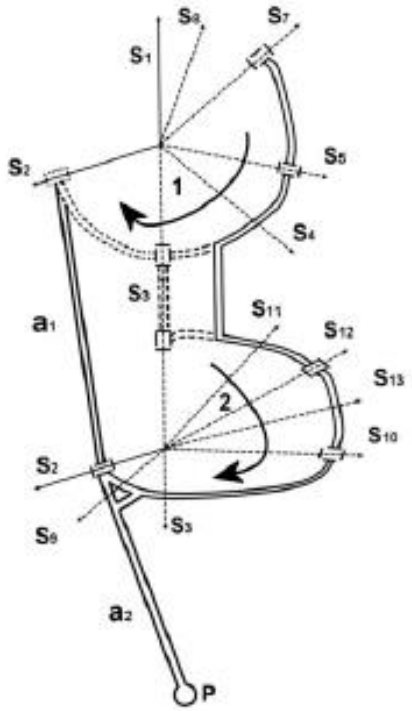

Figure 1: Main principle of overconstrained walking mechanism

The newly designed mechanism is aimed to be operated in a planar plane. To achieve this, as shown in Figure 2a, two revolute joints were initially utilized in the creation of the mechanism, allowing it to execute the desired movements in the plane. In the next stage, the aim was to transfer the motion from the second joint to the body. To accomplish this, two spherical four-bar mechanisms were incorporated into the mechanism initially presented in Figure 2a, as seen in Figure 2b. A common revolute joint was employed by intersecting one of the existing revolute joints. Additionally, the components labeled M1 and M2 in Figure 2a were raised, and these joints were designated as fixed points by attaching motors to them.

In the third stage, with the help of an overconstrained loop structure the joint that had been commonly used was removed to reduce the number of joints and links, as depicted in Figure 2c. Consequently, a double spherical bar linkage with λ equal to five was achieved. However, even in this configuration, two motors were still in use, resulting in two degrees of freedom. To address this, the motors were consolidated to a single location, as shown in Figure 2d. Two additional revolute joints were added at the position of the relocated motor, creating a spherical 4-bar mechanism. As a result, the fundamental principle of the walking mechanism with a single degree of freedom driven by a solitary motor was established.

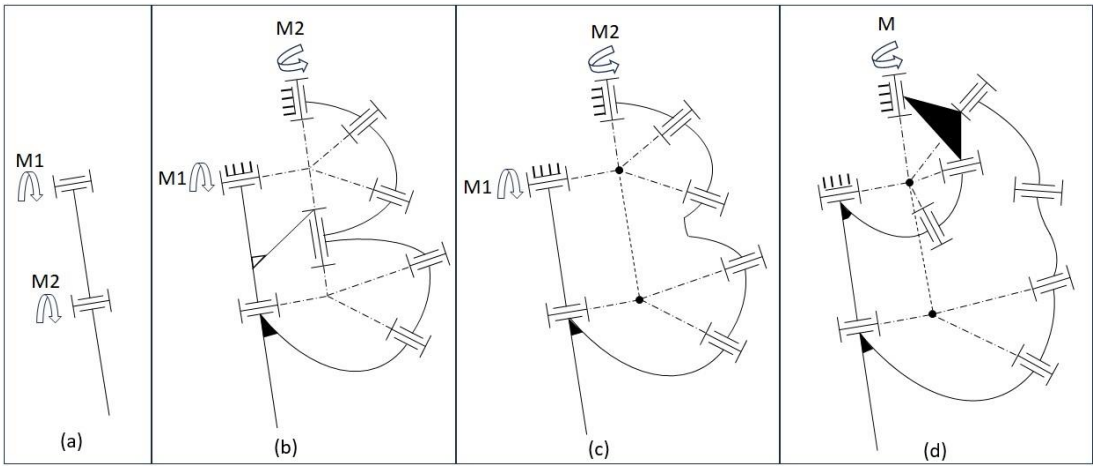

Figure 2: Progress stages of the overconstrained leg mechanism

DoF of the mechanism is calculated for control using Alizade's [37] formula for multi-loop mechanisms with variable subspace numbers.

$$DoF = \sum_{i=1}^{9} f_i - \sum_{i=1}^{2} \lambda_i \quad (2.1)$$

Where the mechanism has two independent loops, the first loop is in a spherical subspace with λ=3, and the second loop is overconstrained with one general constraint loop with λ=5. There are nine revolute joints in the mechanism. Thus, the DoF of the mechanism can be calculated as DoF= 9-(5+3) =1.

2.1 ANALYSIS

In this section, the aim was to conduct both dynamic simulation and kinematic analyses of the mechanism. During the kinematic analysis, the position equations were derived for the endpoint of the mechanism's foot. These equations were then utilized to generate the most suitable walking path by adjusting the lengths of the links. The Mathematica program was used for the creation of these walking paths. The objective was to compare the walking path derived from these position equations with the results obtained from dynamic simulation and experimental tests.

The dynamic simulation was initiated by considering the mechanism as a 6-legged walking robot. Consequently, all the forces acting on the mechanism were calculated. However, all the analysis were made by considering only one leg. The intention was to compare the walking path, acceleration, and speed data to be obtained from the dynamic simulation. The dynamic simulation was performed using the dynamic analysis module of the AutoCAD Inventor program. The methodologies employed in both kinematic and dynamic simulation, the procedure followed, and the utilization of the data acquired are elaborated upon in detail below.

2.1.1 KINEMATIC ANALYSIS

This thesis study involves a kinematic analysis of a mechanism with constant crank rotation, as well as the use of foot position equations to optimize the path. Recurrent unit vector algebra is employed to determine the equations for kinematic calculations. The unit vectors, referred to as "S_i" which describe the joints and links of the mechanism in Figure 3, are calculated using this method [38]. The sequential use of recurrent unit vectors for each loop is shown in Table 1.

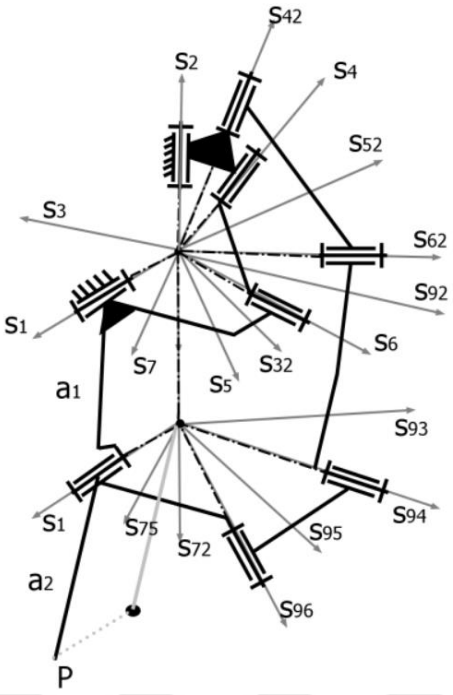

Figure 3: Unit vector representation of the mechanism

To determine the unit vectors for the joints and links of the mechanism depicted in Figure 3 and to use them in the analysis, Equation 2.2 is utilized. The unit vectors S_1 and S_2 are initially attached to the ground link and are placed on the z and x coordinates, respectively, as described in Equation 2.3.

$$S_k = \begin{pmatrix} S_{k.x} \\ S_{k.y} \\ S_{k,z} \end{pmatrix} = \begin{pmatrix} \cos(\alpha_{i,k})S_{i,x} + \sin(\alpha_{i,k})(S_{i,z}S_{j,y} - S_{i,y}S_{j,z}) \\ \cos(\alpha_{i,k})S_{i,y} + \sin(\alpha_{i,k})(-S_{i,z}S_{j,x} + S_{i,x}S_{j,z}) \\ \cos(\alpha_{i,k})S_{i,z} + \sin(\alpha_{i,k})(S_{i,y}S_{j,x} - S_{i,x}S_{j,y}) \end{pmatrix} \tag{2.2}$$

Where $\alpha_{i,k}$is the angle between i^{th} and the k^{th} unit vector.

$$S_1 = \begin{pmatrix} S_{1.x} \\ S_{1.y} \\ S_{1,z} \end{pmatrix} = \begin{pmatrix} 0 \\ 0 \\ 1 \end{pmatrix} \; S_2 = \begin{pmatrix} S_{2.x} \\ S_{2.y} \\ S_{2,z} \end{pmatrix} = \begin{pmatrix} 0 \\ 1 \\ 0 \end{pmatrix} \tag{2.3}$$

For the analysis of the first spherical loop, we use Equation 2.1 for recurrent calculations of other unit vectors, in conjunction with Table 1. With this method, unit

vector s_6 is determined from both sides of the loop and signed with a * if the vector is determined from the other side.

Table 1: Unit vector calculation sequence

	Spherical Loop						Overconstrained First Loop							Overconstrained Second Loop						
Direction	I				II		I				II			I					II	
i	1	2	3	4	2	1	1	2	32	42	2	1	72	2	1	72	93	94	72	1
j	2	3	4	5	1	7	2	32	42	52	1	72	92	1	72	93	94	95	1	73
k	3	4	5	6	7	6^*	32	42	52	62	72	92	62^*	72	93	94	95	96^*	73	96^*

In table

Eliminating $\alpha_{3,5}$ from equality of $s_6 = s_6^*$ and solving for $\alpha_{2,7}$ gives

$$\alpha_{2,7} = Atan2[A, B] \pm \cos^{-1}\left[C/\sqrt{A^2 + B^2}\right] \tag{2.4}$$

Where;

$$A = \cos[\alpha_{1,3}] \sin[\alpha_{1,8}] \sin[\alpha_{2,4}]$$

$$B = -\cos[\alpha_{2,4}] \sin[\alpha_{1,8}]$$

$$C = -(\cos[\alpha_{4,6}] - \cos[\alpha_{1,8}] \sin[\alpha_{1,3}] \sin[\alpha_{2,4}])$$

Then using equality of $s_6 = s_6^*$, $\alpha_{3,5}$ can be found as

$$\alpha_{3,5} = Atan2[\cos(\alpha_{3,5}), \sin(\alpha_{3,5})] \tag{2.5}$$

Where;

$$\sin[\alpha_{3,5}] = \cos[\alpha_{1,8}]\ \csc[\alpha_{4,6}] \sec[\alpha_{1,3}] +$$
$$(-\cot[\alpha_{4,6}] \csc[\alpha_{2,4}] + \cot[\alpha_{2,4}] \csc[\alpha_{4,6}] \sin[\alpha_{1,8}] \sin[\alpha_{2,7}]) \tan[\alpha_{1,3}]$$
$$\cos[\alpha_{3,5}] = \cot[\alpha_{2,4}] \cot[\alpha_{4,6}] - \csc[\alpha_{2,4}] \csc[\alpha_{4,6}] \sin[\alpha_{1,8}] \sin[\alpha_{2,7}]$$

Constants ϕ_1 and ϕ_2 are added to joint angles $\alpha_{1,3}$ and $\alpha_{2,7}$ and $\alpha_{1,32}$ and $\alpha_{2,72}$ are introduced respectively which also will be used in the optimization as construction parameters.

$$\alpha_{1,32} = \alpha_{1,3} + \Phi_1$$
$$\alpha_{2,72} = \alpha_{2,7} + \Phi_2 \tag{2.6}$$

Eliminating $\alpha_{32,52}$ from equality of $s_{62} = s_{62}^*$ and solving for $\alpha_{1,92}$ gives:

$$\alpha_{1,92} = Atan2[D, E] \pm \cos^{-1}\left[F/\sqrt{D^2 + E^2}\right] \tag{2.7}$$

Where;

$$D = \left(-\cos[\alpha_{1,32}]\cos[\alpha_{2,72}]\sin[\alpha_{2,42}] + \cos[\alpha_{2,42}]\sin[\alpha_{2,72}]\sin[\alpha_{72,82}]\right)$$

$$E = \left(-\sin[\alpha_{1,32}]\sin[\alpha_{2,42}]\sin[\alpha_{72,82}]\right)$$

$$F = -\Big(\cos[\alpha_{42,62}] - \cos[\alpha_{72,82}]\left(\cos[\alpha_{2,42}]\sin[\alpha_{2,72}] + \cos[\alpha_{1,32}]\sin[\alpha_{2,42}]\sin[\alpha_{2,72}]\right)\Big)$$

Similar to spherical loop $\alpha_{32,52}$ can be found from equality of $s_{62} = s_{62}^*$ from the first imaginary spherical loop of the overconstrained loop.

$$\alpha_{32,52} = Atan2\left[\sin(\alpha_{32,52}), \cos(\alpha_{32,52})\right] \tag{2.8}$$

Where;

$$\sin[\alpha_{32,52}] = -\csc[\alpha_{42,62}]\left(\cos[\alpha_{72,82}]\sin[\alpha_{1,32}]\sin[\alpha_{2,72}] + \left(\cos[\alpha_{1,92}]\cos[\alpha_{2,72}]\sin[\alpha_{1,32}] - \cos[\alpha_{1,32}]\sin[\alpha_{1,92}]\right)\sin[\alpha_{72,82}]\right)$$

$$\cos(\alpha_{32,52}) = \csc[\alpha_{42,62}]\sec[\alpha_{2,42}]\sin[\alpha_{1,32}]\sin[\alpha_{1,92}]\sin[\alpha_{72,82}] + \cos[\alpha_{1,32}]\csc[\alpha_{42,62}]\sec[\alpha_{2,42}]\left(\cos[\alpha_{72,82}]\sin[\alpha_{2,72}] + \cos[\alpha_{1,92}]\cos[\alpha_{2,72}]\sin[\alpha_{72,82}] + \cos[\alpha_{1,92}]\cos[\alpha_{2,72}]\sin[\alpha_{72,82}]\right) - \cot[\alpha_{42,62}]\tan[\alpha_{2,42}]$$

$\alpha_{1,93}$is introduced adding Φ_3 to $\alpha_{1,92}$

$$\alpha_{1,93} = \alpha_{1,92} + \Phi_3 \tag{2.9}$$

Eliminating $\alpha_{93,95}$ from equality of $s_{96} = s_{96}^*$ and solving for $\alpha_{72,73}$ gives:

$$\alpha_{72,73} = Atan2[G, H] \pm \cos^{-1}\left[J/\sqrt{G^2 + H^2}\right] \tag{2.10}$$

Where;

$$G = -\cos[\alpha_{72,94}]\sin[\alpha_{1,74}]$$

$$H = \cos[\alpha_{1,93}]\sin[\alpha_{1,74}]\sin[\alpha_{72,94}]$$

$$J = -\left(\cos[\alpha_{94,96}] - \cos[\alpha_{1,74}]\sin[\alpha_{1,93}]\sin[\alpha_{72,94}]\right)$$

Similar to spherical loop $\alpha_{93,95}$ can be found from equality of $s_{96} = s_{96}^{*}$ from the second imaginary spherical loop of the overconstrained loop.

$$\alpha_{93,95} = Atan2\left[\sin\left(\alpha_{93,95}\right), \cos\left(\alpha_{93,95}\right)\right] \tag{2.11}$$

Where;

$$\sin\left[\alpha_{93,95}\right] = \Big(\csc\left[\alpha_{94,96}\right]\Big(\sin\left[\alpha_{1,93}\right]\left(\cos\left[\alpha_{2,72} + \alpha_{72,73}\right]\cos\left[\alpha_{72,94}\right]\sin\left[\alpha_{1,74}\right] + \cos\left[\alpha_{94,96}\right]\sin\left[\alpha_{2,72}\right]\right) + \cos\left[\alpha_{1,74}\right]\left(\cos\left[\alpha_{1,93}\right]\cos\left[\alpha_{2,72}\right]\cos\left[\alpha_{72,74}\right] - \sin\left[\alpha_{2,72}\right]\sin\left[\alpha_{72,94}\right]\right)\Big)\Big)\left(\cos\left[\alpha_{2,72}\right]\cos\left[\alpha_{72,94}\right] - \cos\left[\alpha_{1,93}\right]\sin\left[\alpha_{2,72}\right]\sin\left[\alpha_{72,94}\right]\right)^{-1}$$

$$\cos\left[\alpha_{93,95}\right] = \Big(\csc\left[\alpha_{94,96}\right]\sec\left[\alpha_{72,94}\right]\left(-\cos\left[\alpha_{2,72} + \alpha_{72,73}\right]\cos\left[\alpha_{72,94}\right]\sin\left[\alpha_{1,74}\right] + \cos\left[\alpha_{1,74}\right]\cot\left[\alpha_{2,72}\right]\tan\left[\alpha_{1,93}\right]\right) - \cot\left[\alpha_{94,96}\right]\left(1 + \cot\left[\alpha_{2,72}\right]\sec\left[\alpha_{1,93}\right]\tan\left[\alpha_{72,94}\right]\right)\Big)\left(\cot\left[\alpha_{2,72}\right]\sec\left[\alpha_{1,93}\right] - \tan\left[\alpha_{72,94}\right]\right)^{-1}$$

$\alpha_{72,75}$ is introduced by adding Φ_4 to $\alpha_{72,73}$

$$\alpha_{72,75} = \alpha_{72,73} + \Phi_4 \tag{2.12}$$

$\alpha_{2,72}$ and $\alpha_{72,75}$ are used to find the position change of the path point P (P_x P_y) as shown in Equation.

$$P_x = a_1 * \cos\left[\alpha_{2,72}\right] + a_2 * \cos\left[\alpha_{2,72} + \alpha_{72,73}\right]$$
$$P_y = a_1 * \sin\left[\alpha_{2,72}\right] + a_2 * \sin\left[\alpha_{2,72} + \alpha_{72,73}\right] \tag{2.13}$$

P_x and P_y define the path of the end of the leg concerning input $\alpha_{1,3}$, which will be used later in the optimization of the link lengths for a desired strider length and step height. If we define $a_1 = k_1 * L$ and $a_2 = k_2 * L$, equation (2.13) shows that the path is independent of the radius of the spherical links; thus, they can independently be scaled without affecting the kinematic characteristic of the mechanism.

2.1.2 DYNAMIC SIMULATION

Walking mechanisms must draw a straight line as much as possible in the x-axis direction when touching the ground to move. This is done by dynamically simulating the models drawn in the CAD (Computer Aided Design) program with the help of Inventor. Dynamic simulation is used in two stages. First, the second interval during which the mechanism draws a straight line is determined. Then, the loads in the region corresponding to this time interval are entered into the system.

Several methods can be used to determine which seconds the mechanism draws a straight line. These can be read as the region where the velocity on the Y axis is the flattest or the region where the Y value is constant from the position graph. The velocity graph of a walking mechanism in the Y-axis is shown below, depending on time. From Figure 4, it can be assumed that the mechanism draws a straight line between 1.7t and 3.6t.

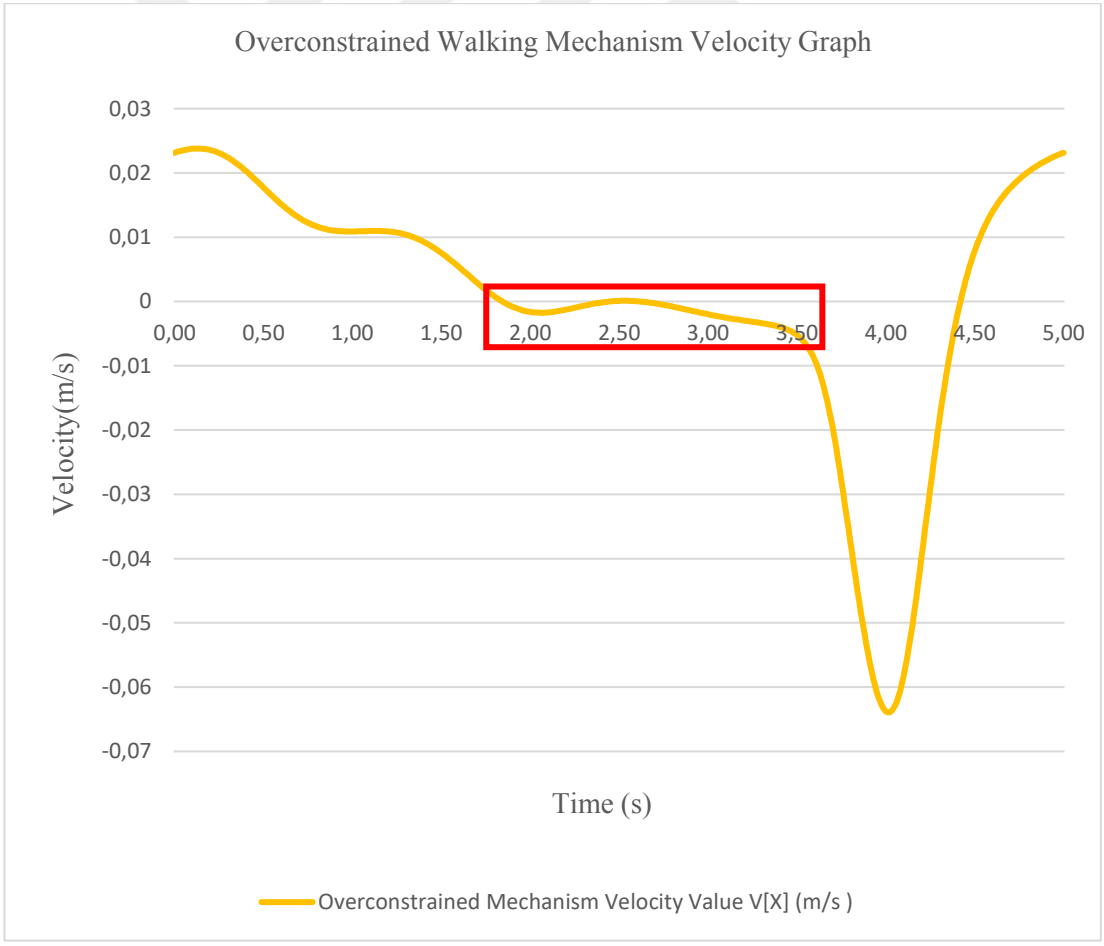

Figure 4: Velocity of point P in X direction

After this stage, the necessary forces in the X and Y directions were entered into the program, as we knew between which seconds the mechanism drew a straight line. The weight values in Table 2 below were used when entering the forces in the X direction. Since there is a single experimental setup. It was assumed that these values were the same in other walking mechanisms.

The force on the Y axis was determined by using the material whose coefficients we know, instead of finding the coefficient of friction between the material produced from the 3D printer and the test equipment material, plexi glass. For this reason, a value in the middle of the coefficients between rubber-rubber and plexiglass-plexiglass materials was taken. In this way, the friction force was assumed.

Table 2: Friction force parameters and calculation

Part Name	**Quantity**	**Weight Per Each Member (kg)**	**Total Weight (kg)**	**Weight per Each Mechanism (kg)**	**Friction Coefficient (Rubber-Plexiglass)**	**Friction Force (N)**
Motor	6	0,150	0,900	0,300		
Arduino	1	0,025	0,025	0,008		
Cover Box, Top Plate and Bottom Plate	1	1,251	1,251	0,417		
Bread Board	2	0,050	0,100	0,033		
Cables and motor driver	1	0,020	0,020	0,007		
Power Supply	1	0,215	0,215	0,072		
Body	6	0,340	2,040	0,680		
			3,651	1,217	0,9	10,745

As seen in Figure 5, between 0 and 1.7 seconds in the X direction, the force is zero since the mechanism does not touch the ground. But after 1.7 seconds, the force increases to 12 Newtons as the mechanism hits the ground. For 1.9 seconds, the force the mechanism applies remains constant, and then the force becomes zero.

The same is true for Fy, as shown in Figure 6. The force is 0 in the regions where the mechanism does not step on the ground and 10.7 N in the areas where it does.

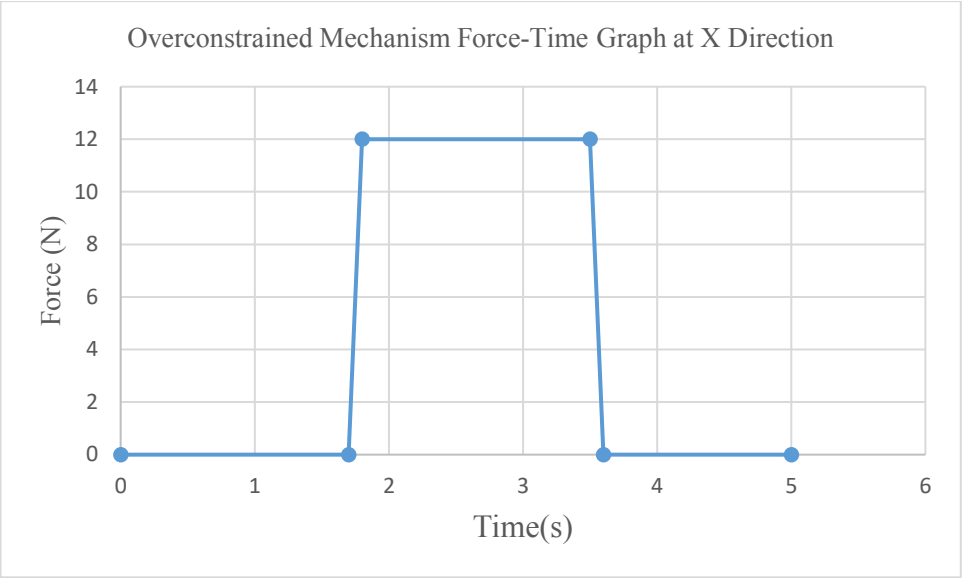

Figure 5: Force-Time graph at X direction

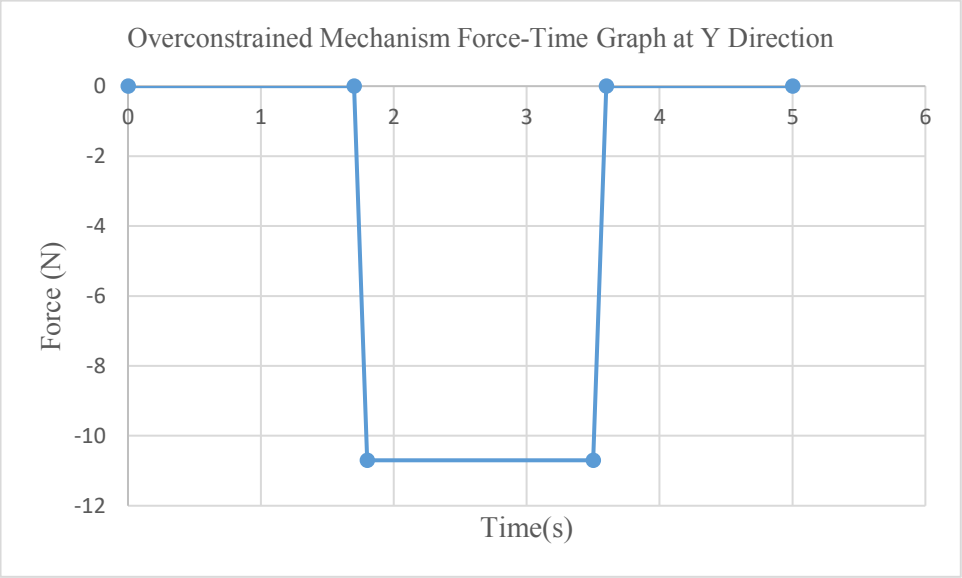

Figure 6: Force-Time graph at Y direction

After all the forces acting on the mechanism were entered into the simulation, acceleration, speed and torque values were obtained.

The purpose of obtaining velocity values was to compare the velocity values that would be obtained from the test setup. The purpose of determining the torque values is to compare our mechanism with other mechanisms. The major aspects at this section are the fluctuations in speed and torque the average torque and force values in motion.

2.2 LEG TRAJECTORY FOR WALKING MECHANISMS.

The path at the end of the foot is called the locus. The locus consists of 4 stages as shown in Figure 7. These are driving, lifting, turning, and lowering. During the driving phase the foot is in contact with the ground and carries the weight of the body. In the lifting phase, the leg is lifted to overcome any obstacle and is crossed in the turning phase. The height of the obstacle it can pass is called the step height. Finally, the foot touches the ground again.

The kinematic analysis resulted in 8 different path combinations. The combinations consist of alternative results of equations (2.4), (2.7), and (2.10). The walking paths obtained from alternative results are as shown in Table 3. In the table + and - in the configuration section represent the sign at the beginning of the mentioned equations. Each of the lines in the Trial Result section is defined as 100 mm. Later the combination with (+++) is selected for construction due to its stride to height of the step ratio, stride to leg height ratio. The parameters of the +++ configuration selected in Table 3 are as shown in Table 4.

Table 3: Alternative solution configurations

Configuration	+ + +	+ + -	+ - +	- + +
	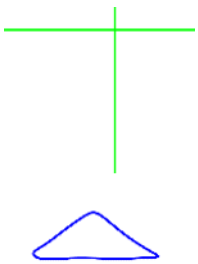	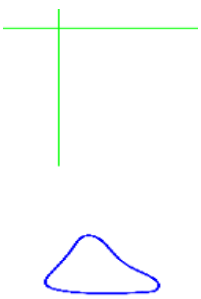		
Configuration	+ - -	- + -	- - +	- - -
		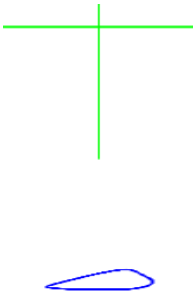		

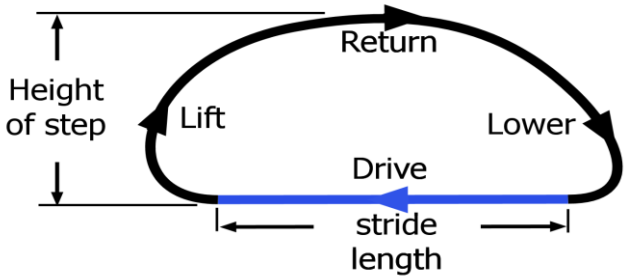

Figure 7: Locus of a leg mechanism

Table 4: Link dimensions by trial

Parameters	$\alpha_{2,4}$	$\alpha_{4,6}$	$\alpha_{1,8}$	$\alpha_{72,82}$	$\alpha_{2,42}$	$\alpha_{42,62}$	$\alpha_{72,94}$	$\alpha_{94,9}$
Trial Value	15°	117°	113°	141°	286°	98°	11°	46°
Parameters	$\alpha_{1,74}$	Φ_1	Φ_2	Φ_3	Φ_4	a_1	a_2	
Trial Value	58°	342°	0°	1°	24°	100 mm	100 mm	

CHAPTER III

TEST SETUP

The aim of the test setup was to verify the correct operation of the mechanism and ensure the accuracy of the data obtained from the dynamic simulation.
The moving plate assembly was designed to demonstrate the proper operation of the mechanism. The design of the test setup was carried out using the SolidWorks program. Plexiglass materials, with a thickness of 5 mm, were chosen due to the presence of a moving structure. Transparent materials were selected to provide a clear view of the mechanism during the analysis.

From an electronic standpoint, achieving the accuracy of the dynamic simulation could be accomplished through various methods. It can be stated that the determination of the measurement method played a critical role in the creation of the test setup, impacting both electronic and structural aspects. Therefore, before the test setup was created, decisions were made regarding the data that would be obtained from the dynamic simulation, along with the selection of the desired materials and their respective positions.

3.1 CAD DESIGN FOR TEST SETUP

The plexiglass parts of the test setup consist of 5 parts as seen in figure 8. Technical drawings of the parts produced from plexiglass and 3D printer are given in the appendix.

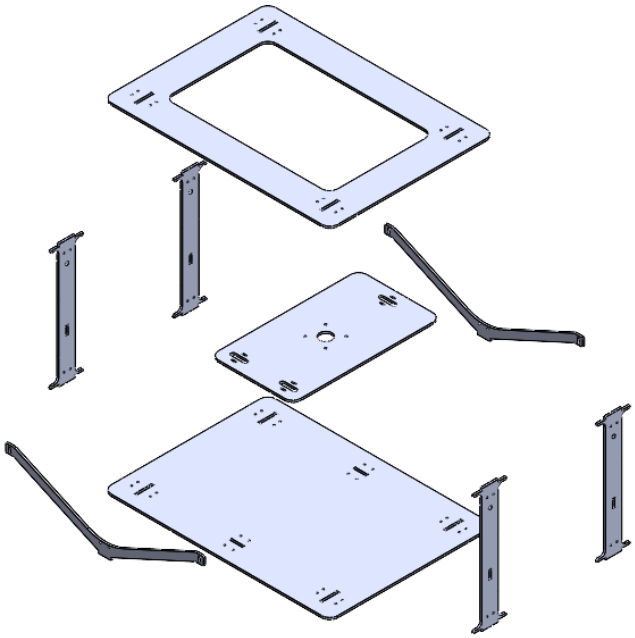

Figure 8: Exploded view of test setup's plexiglass parts

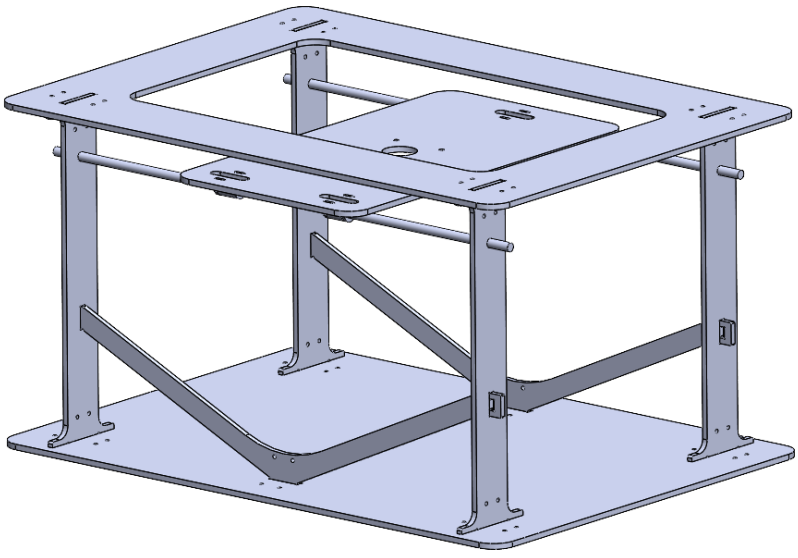

Figure 9: Assembled test setup's frames and rods

3.2 SETTING UP THE TEST SETUP

The parts and their quantities used in creating the test setup are shown in Table 5. The test setup was completed in 2 stages. These are mechanical and electronical.

Table 5: Part list of test setup

Part Name	Quantity
Nema 17 Motor	1
Arduino	1
Bottom Plexiglass	1
Top Plexiglass	1
Plexiglass Plate (movable)	1
Plexiglass Column	4
Plexiglass V Shape	2
Bread Board	2
Step Motor Driver	1
Cables (Jumper)	16
Adaptor (Square 3D Plate)	2
Tripod	1
Caplin	1
Rubber Tape	1
Power Supply 12V 1A	1
Fastener M3x20	20
Fastener M3x16	20
Nut	40
Washer	32
Gridded Background	1

3.2.1 MECHANICAL SETUP

In this part, plexiglass material was used so that everything could be seen clearly during the movement of the mechanism. Given that the sharp corners are subject to stress during the cutting of plexiglass materials, it was designed to be suitable for plexiglass cutting techniques, as shown in Figuren 10. ±0.1 mm tolerance was given for interlocking parts.

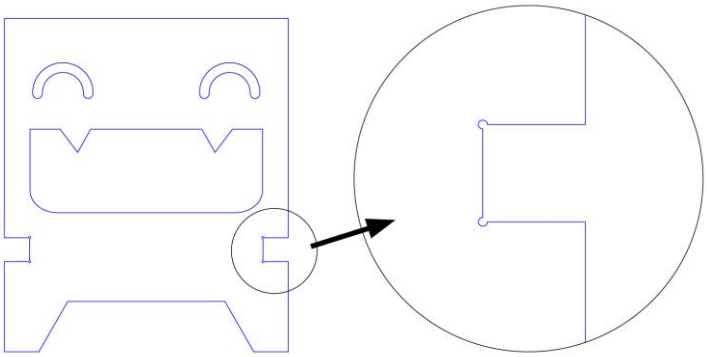

Figure 10: Plexiglass cutting method

The assembly of the test setup started by assembling the plexiglass components. L brackets printed from a 3D printer were used to make the assembly more stable. Only nuts, bolts, and washers were used in the assembly of all mechanical parts. After the main structure was assembled, the assembly of the moving components, which is necessary for the mechanism to walk, was completed. Three linear bearings were installed for easy movement of the plate. Linear bearings were fixed on the moving plate with a plastic clamp. After completing the assembly of the moving plate, spacers produced from the intermediate 3d printer were used to assemble the mechanism. These spacers were designed to adjust the height of the motor.

3.2.2 ELECTRONICAL SETUP

The aim of this part is to achieve control of the motor's desired speed and direction while collecting the required test data. To fulfill this objective, a code was generated for use with Arduino. Within the code, options for controlling the engine, including direction (CW and CCW) and stopping, were incorporated, making it possible to manage the mechanism's motion in the intended direction and halt it at will through the serial monitor.

NEMA17 series stepper motor was used to actuate the mechanism, and a DRV8825 step motor driver was utilized to achieve the desired motor operation as shown in Figure 11 [39]. A potentiometer is available on the motor driver, allowing for curret adjustment. This adjustment affords the opportunity to augment the current when the motor's power proves insufficient. The utilization of a stepper motor stems from its capability to deliver high performance even under conditions of minimal sensitivity

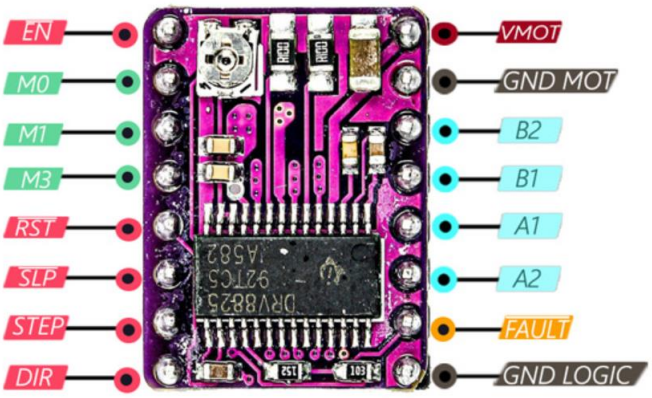

Figure 11: DRV8828 step motor driver

3.2.2.1 Circuit Schema

The RST and STP legs of the motor driver are connected to the 5V and GND ports of the Arduino, and the STEP and DIR legs are connected to ports 3 and 2 of the Arduino respectively. When we look at the pins of the motor from the left side, pins 1, 3, 4, and 6 are connected to pins B2, B1, A1, and A2 respectively. VMOT and GND MOT are connected to the + and - poles of the power supply respectively. The wiring diagram is shown in Figure 12 [39].

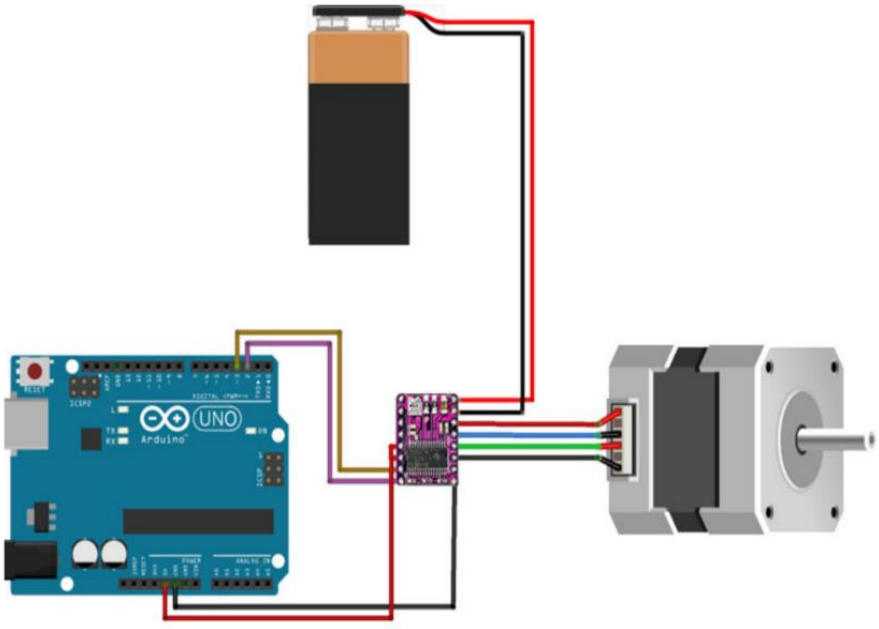

Figure 12: Interfacing DRV8825 step motor driver with Arduino

3.2.2.2 Digital Image Processing

Instead of using a sensor to get data from the mechanism since the engine was running, it was aimed to extract the end effector speed and walking path of the mechanism by taking frame-by-frame images from the video with the "Digital Image Correlation" method.

For this purpose, a 60 fps video camera was recorded to see the mechanism directly from the front. This video recording was converted into photographs. It was aimed to extract speed graphs from the photographs obtained from the video recording, knowing the time and location.

3.3 ASSEMBLY OF THE TEST SETUP

The main structure was assembled parts cut from plexiglass and materials produced by a 3D printer as shown in Figure 13.

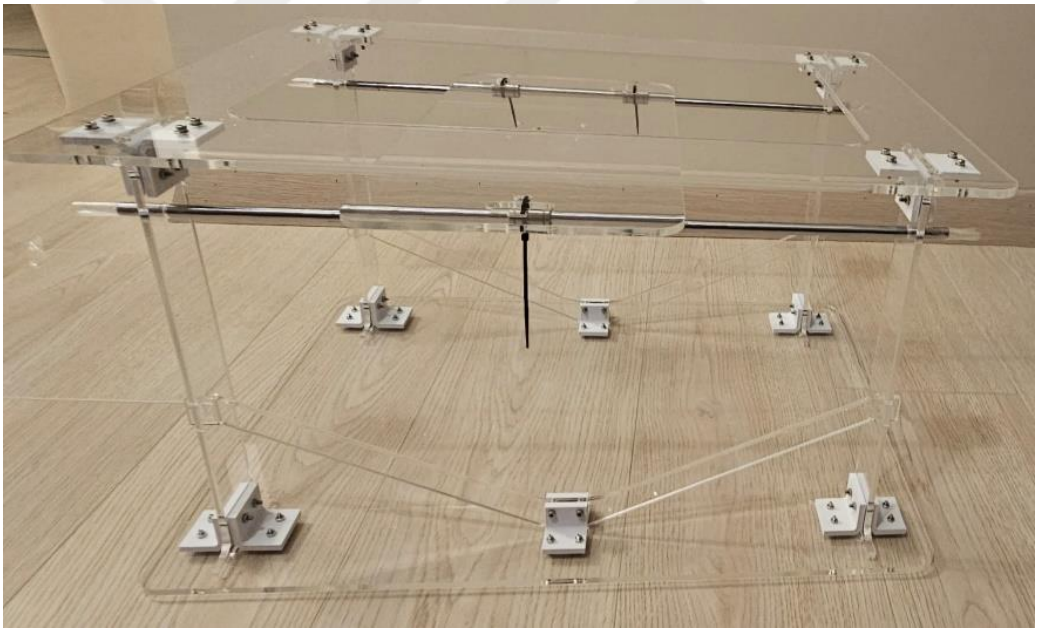

Figure 13: Main body of the test setup

The square 3D printed plate and the caplin were assembled to the proposed overconstrained mechanism, as shown in Figure 14.

Figure 14: Plate and caplin assembly to mechanism

The walking mechanism and the square plate produced with the 3D printer were assembled to the moving plate, as shown in Figure 15.

Figure 15: Mechanism assembly to moving plate

The plate that will hold the motor was attached to the motor and nuts were placed in between for height adjustment, as shown in Figure 16.

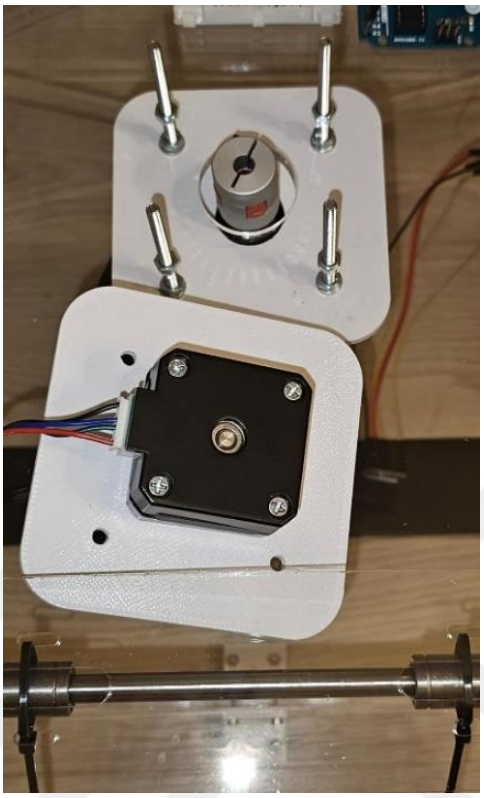

Figure 16: Assembly of the motor

The circuit board, Arduino, tripod, cables, and background were placed according to the most suitable position, as shown in Figure 17.

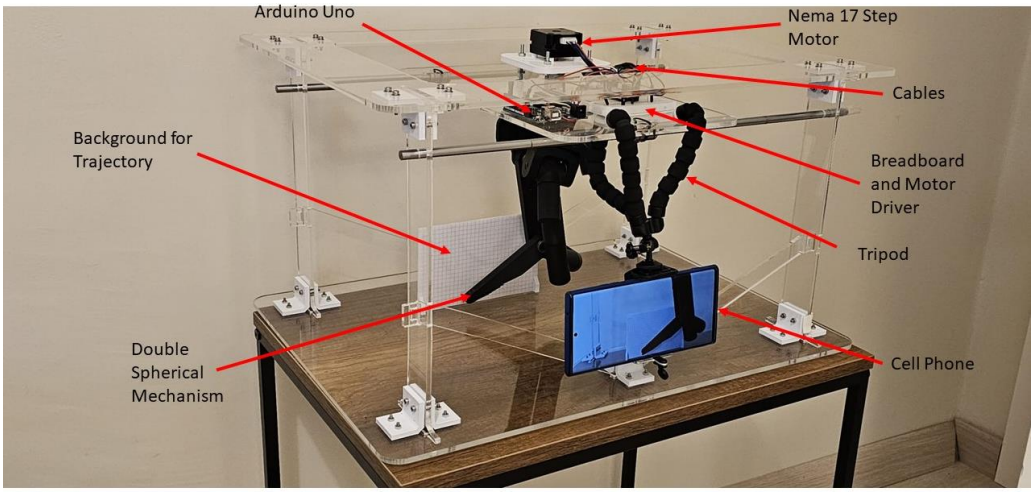

Figure 17: Assembled test setup

A rubber band was glued to the end of the foot, as shown in Figure 18.

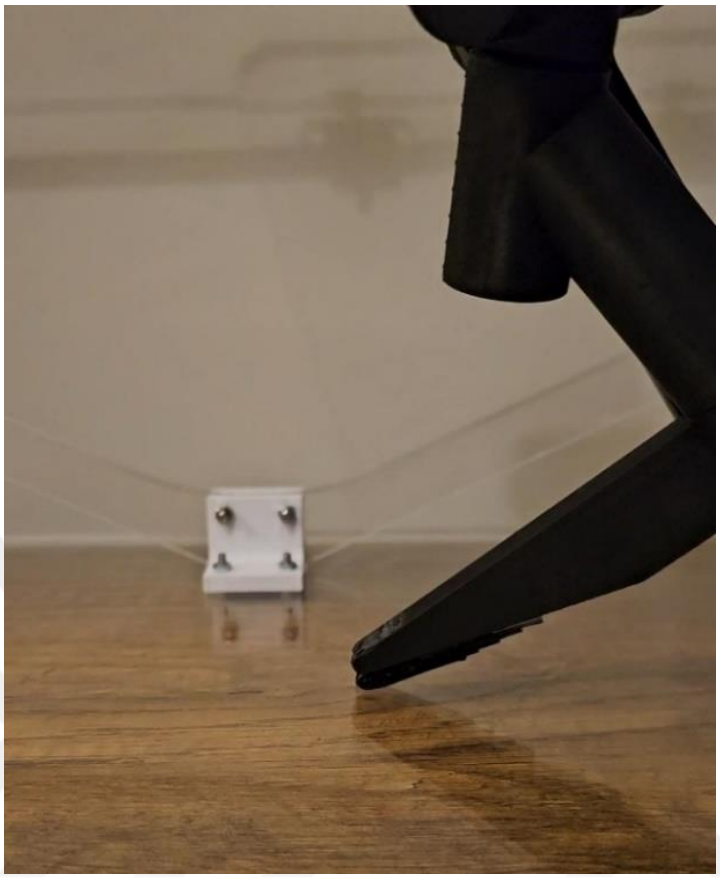

Figure 18: Rubber band assembly

3.4 IMPLEMENTATION OF THE TEST

One of the important factors when recording video in the test setup is that the camera is facing straight ahead and a reference measurement is used. For this reason, a 3D-printed part was created to act as a screen at the back of the mechanism. On top of this part, a square of paper with known dimensions was placed, each square being 5x5 mm, to facilitate reading the velocity (Figure 19).

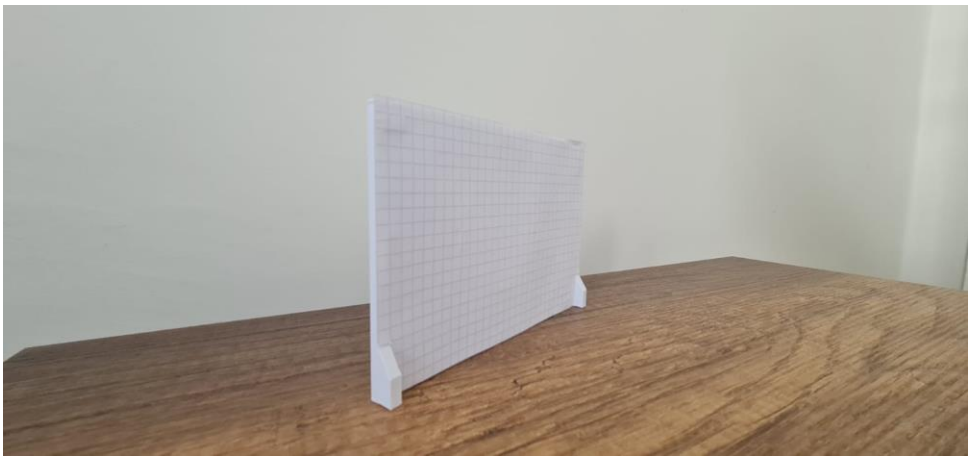

Figure 19: Background for test mechanism

During the operation of the mechanism, a tripod was used to keep the camera aligned with the mechanism, as seen in Figure 20. In order to verify the angle of the camera and get as accurate results as possible, it was calibrated using the gyroscope inside the phone.

Figure 20: Tripod assembly to test setup

After this stage, the speed can be calculated since the time and position change between the images taken from the video recording are known. In Figure 21, two different images of the mechanism in motion are superimposed on top of each other. The interval between these two frames was measured as 0.1 seconds. The difference between the photos is 1.5 square, so the distance is 7.5-7.7 mm. This allows the speed in this time interval to be calculated.

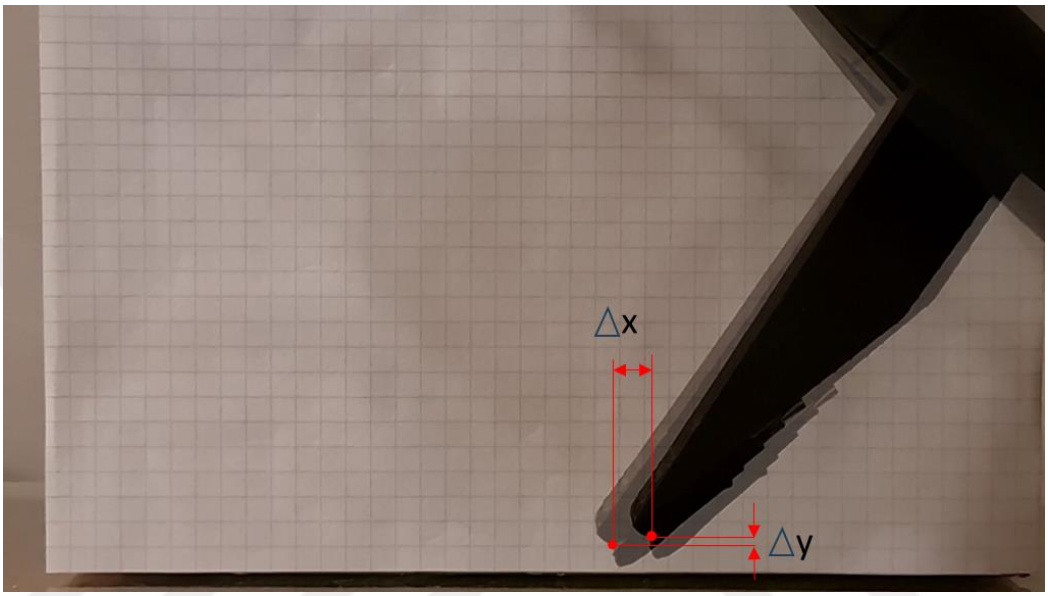

Figure 21: Velocity calculation method

CHAPTER IV

RESULTS

This section aims to compare the data obtained from the dynamic simulation and test setup we have made. It is aimed to explain and prove the differences in the comparisons in a scientific way. The results section is explained in two parts. These are test results and dynamic simulation. The test results were based on the evaluation of the experimentally obtained data of the mechanism. The dynamic simulation section, is aimed to compare all mechanisms in terms of torque values and to find out which mechanism is the most stable.

4.1 DYNAMIC SIMULATION RESULT

The resultant path of the mechanism is shown in Figure 22a. The drive phase of the leg is between 170˚-50˚ input of the crank. The Lift phase is between 270˚-50˚. The return phase is between 235˚-270˚. The lowering phase is between 170˚-235˚. The path is almost symmetrical concerning the y-axis. In the drive phase during the stride, it is seen that the y motion is nearly straight. The foot trajectory is also drawn in CAD software and simulated. The comparison with the curve drawn with the analytical solution verifies the result (Figure 23).

Since the increments between the independent variable times are equal, the Richardson Method is used for the numerical differentiation. The velocity diagram in Figure 22b shows that velocity in the y-direction is almost zero during the drive phase desired in the lift, and in the lower phases, the jerk is high. In the drive phase, the jerk has a low variation (Figure 22d). At the same time, the end is in the lowering phase between 0˚-50˚. During the lowering phase, acceleration is low. Thus, the undesirable chance of impact to the ground is softer.

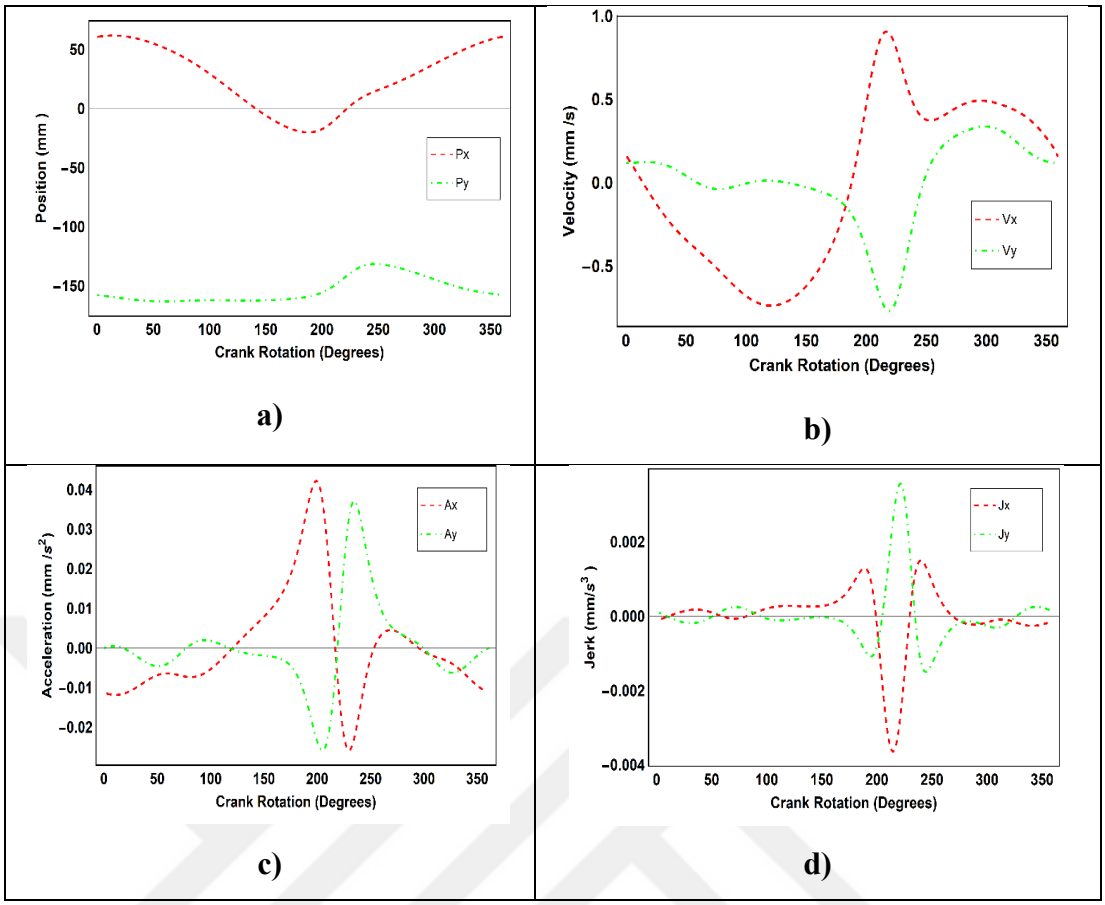

Figure 22: Kinematic results in x and y direction with respect to crank rotation; a) Position, b) Velocity, c) Acceleration, d) Jerk

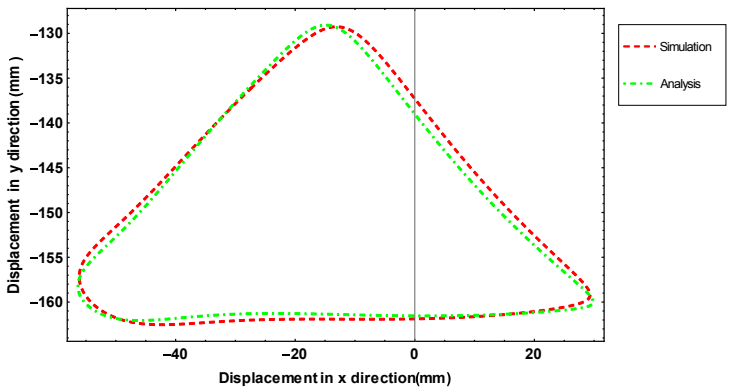

Figure 23: Simulation and analysis result comparison

As seen in Figure 24, the overconstrained walking mechanism is scaled as x1, x2, x4, and x8 respectively. While scaling, the dimensions defined as aa1 and aa2 in the mechanism were scaled up or down at the same rate. As the mechanism is scaled up or down at different scales, the walking path increases or decreases at the same rate.

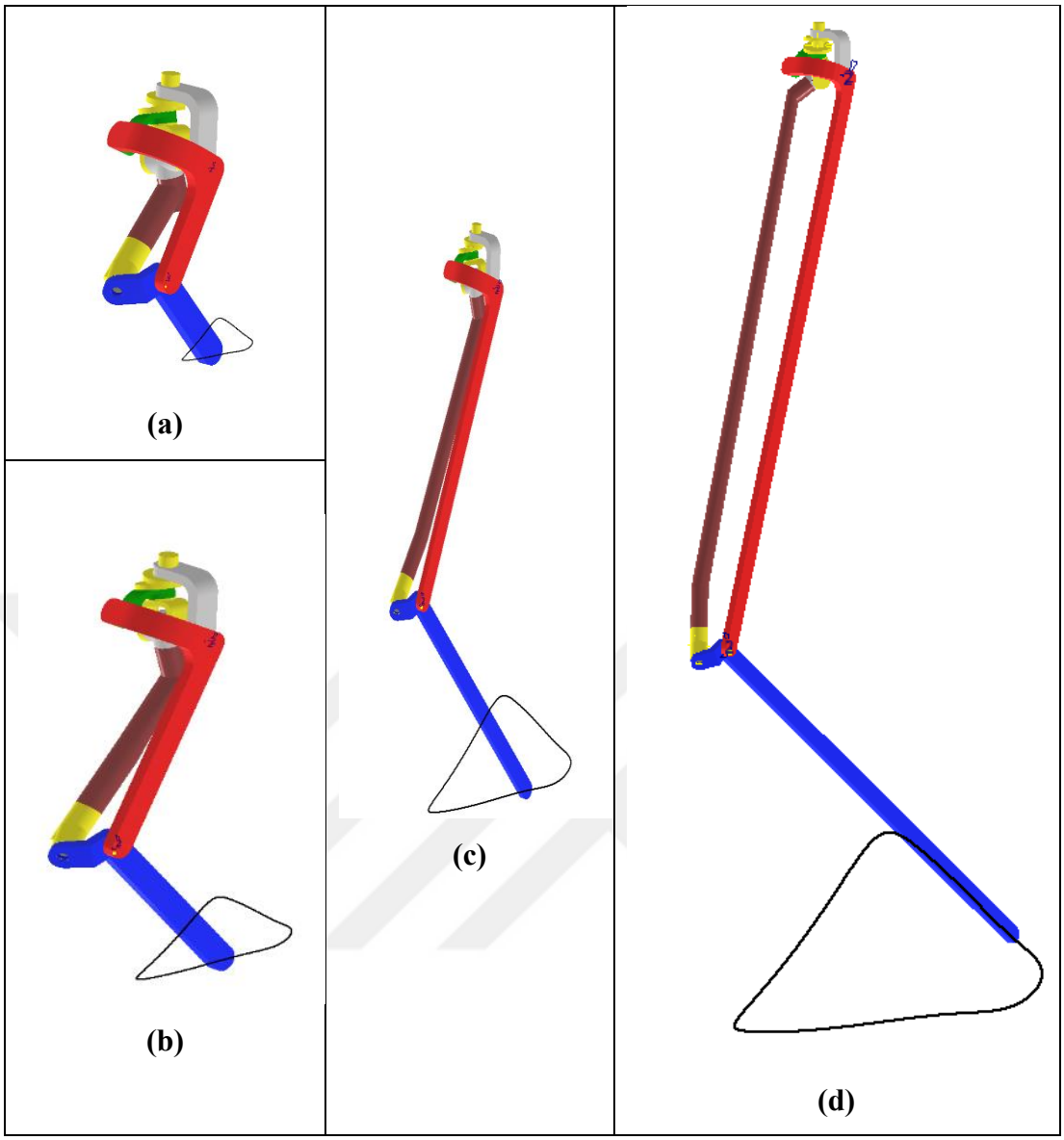

Figure 24: Scaled configurations of the resulting mechanism

The walking paths of the different scaled overconstrained walking mechanisms shown in Figure 24 on the coordinate plane are as shown in Figure 25. Looking at this graph, the walking path increases or decreases in direct proportion to the scaling implemented.

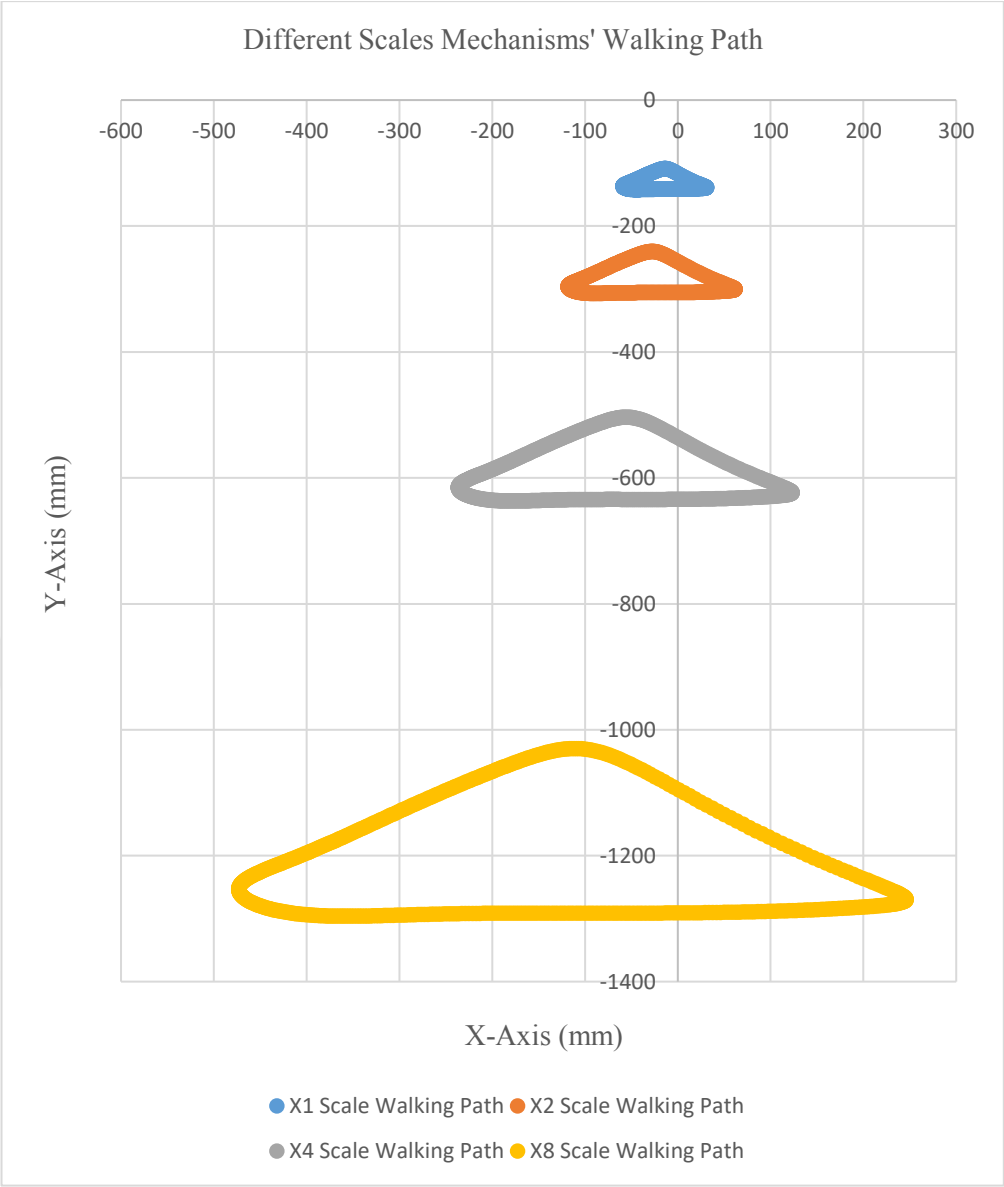

Figure 25: Scaled mechanisms' walking path

Figure 26 shows the torque graph obtained for the overconstrained mechanism. According to the torque graph, the force is zero at first, which indicates that the P point of the mechanism, i.e. the end part of the foot, is in the air in the initial state. 1.7 seconds after the motor starts to move, torque is applied for about two seconds when the foot of the mechanism touches the ground. The desired torque value at the top point of the mechanism is approximately 0.52 N.m. The position of the mechanism when it reaches this value is shown in Figure 27. reaches this value is shown in Figure 27.

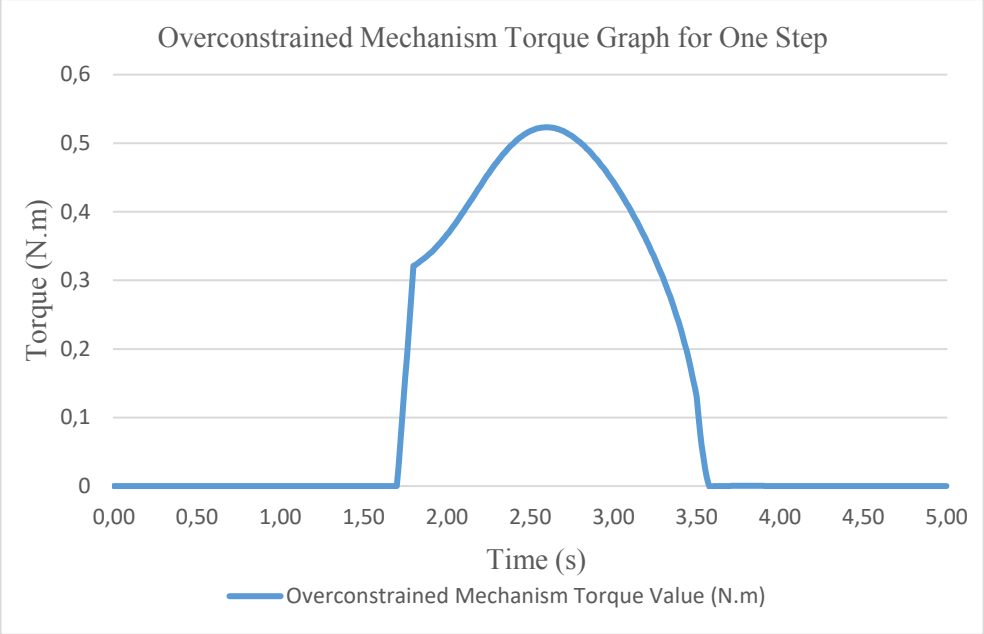

Figure 26: Overconstrained mechanism torque graph

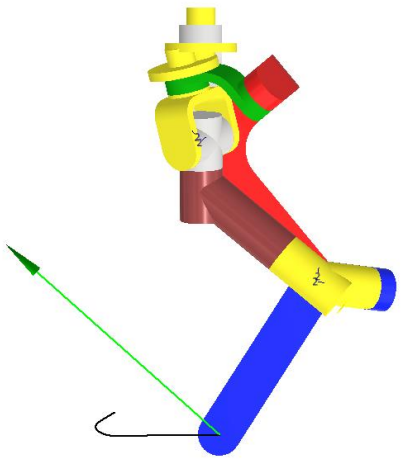

Figure 27: Maximum torque value position

4.2 TEST RESULT

Prior to checking the numerical accuracy of the experimental setup, the walking path obtained previously was checked. As shown in Figure 28, the walking path of the mechanism drawn in the CAD environment and the walking paths obtained in the test environment are exactly the same. Another reason for checking this is that the mechanism actually has more than one walking path. After confirming that the mechanism was in the correct position, the data obtained from the tracker was compared. At the end of the test, the data obtained from dynamic simulation and the data obtained experimentally matched each other.

Figure 28: Mechanism motion frame by frame

The walking path of the mechanism, which is proven to be in the correct position, obtained by the tracker method is shown in Figure 29. When compared with

the walking paths obtained from simulation and analysis in Figure 23, it can be said that the walking path of the mechanism obtained as a result of the test is very close to them.

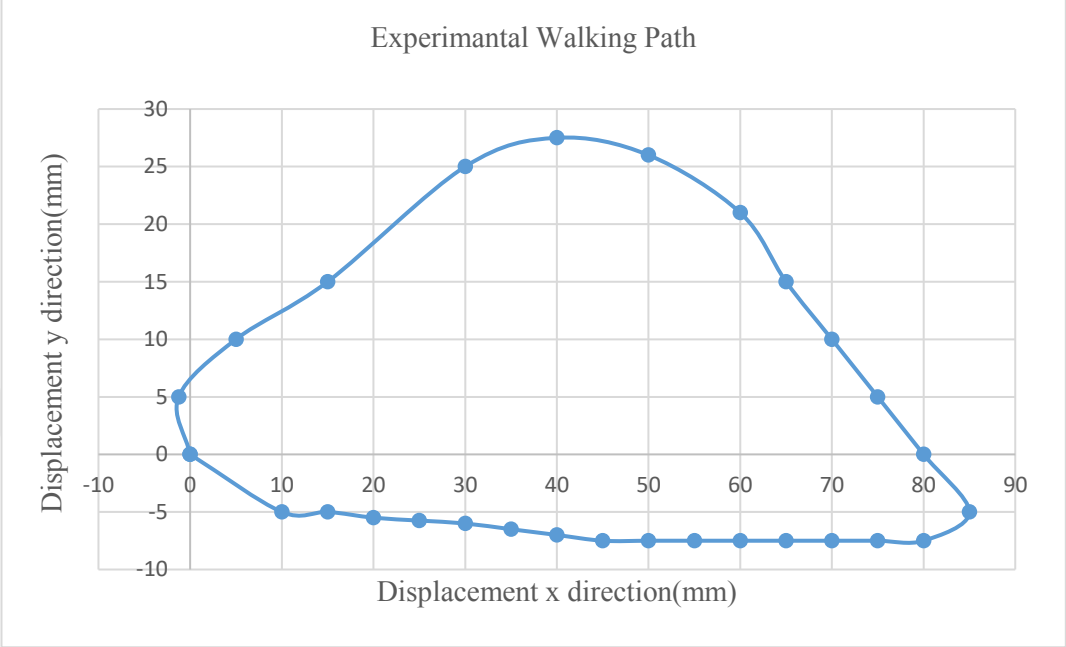

Figure 29: Experimental walking path

There are several reasons for the differences between the walking paths. Production errors, and errors in the measuring devices are the main ones. Although the mechanism was produced on high-precision 3D printers, the design gaps given during the design phase are too large. The large design gaps caused a lot of oscillations during the movement of the mechanism. These oscillations also affected the comparison of the speed graphs obtained from the dynamic simulation of the mechanism.

When examining Figure 30 and Figure 31, the speed graphs obtained from the dynamic simalutions are shown. A general observation from comparing these two graphs is that they exhibit a similar tendecy. However, it becomes apparent that the data collected during the experiment was notably inadequate. This insufficiency in data collection can be attributed as the primary cause for the disparity observed in the dynamic simulation results. The emergence of these differences in the graphs can be attributed to a combination of insufficient data and other errors. Despite these challenges, the data acquired still corroborates the dynamic simulation of the mechanism.

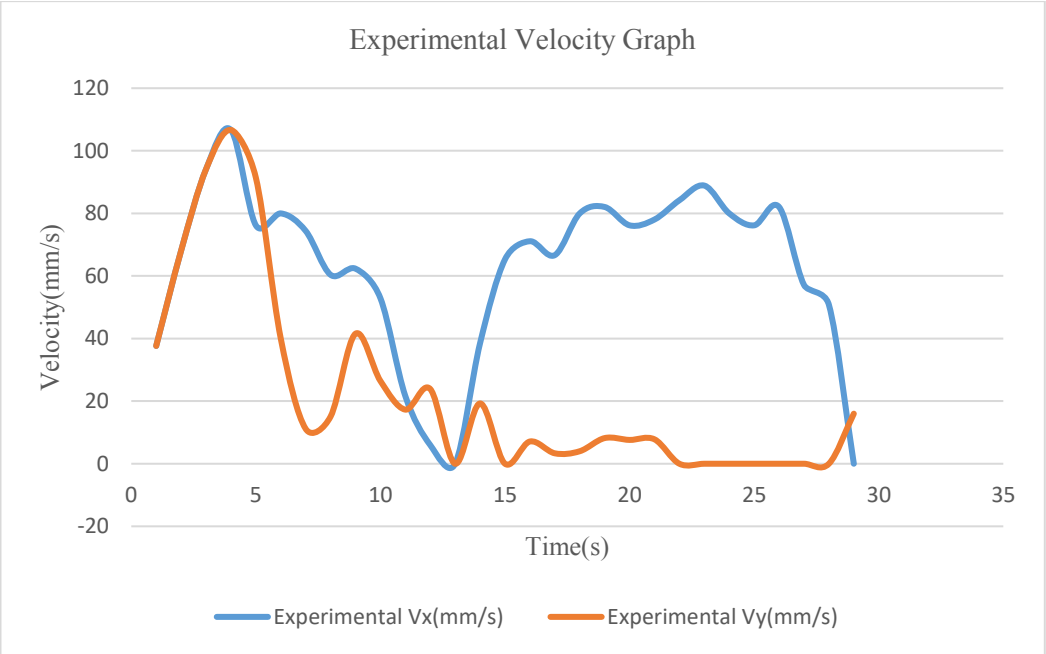

Figure 30: Test setup results for velocity

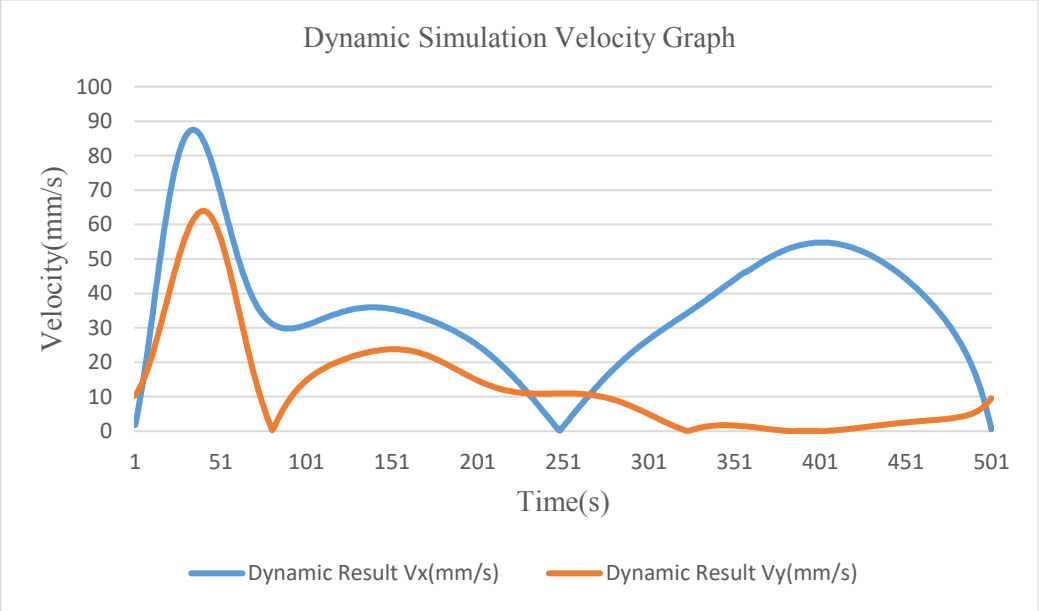

Figure 31: Dynamic simulation results for velocity

Assuming that the data obtained from the experiment was correct, a separate test mechanism was not established for other mechanisms. A comparison of the dynamic simulation results of the designed mechanism with the other mechanisms was made using Autocad Inventor.

CHAPTER V

DISCUSSION

To observe the differences between the walking mechanisms in the literature and the possible benefits of the proposed overconstrained mechanism, a comparison table is shown in Table 6. The comparison subjects were determined by considering the areas of use, assembly, and intended use of the mechanisms.

1. Number of Links: It refers to the number of links used during the design of the mechanisms.
2. Number of Joints: It refers to the joints used between the links of the mechanisms.
3. Number of the Supports on The Frame: In order for the mechanism to make the desired movement in the desired plane, it must be fixed from a minimum of two points. This section shows how many points the mechanism is fixed.
4. Scalable: In the movement of the mechanisms, the P point (the end part of the mechanism) creates a path. In order to increase or decrease this path, the whole mechanism must be scaled. Only in the overconstrained mechanism, the dimensions of the path can be changed without scaling the whole mechanism.
5. Stride Length Proportion to Body Size: It is the ratio of the distance that the mechanism is considered to be walking, i.e., walking in a straight line, to the length of the mechanism. This ratio is changeable due to the scalability of the overconstrained mechanism (Figure 32).

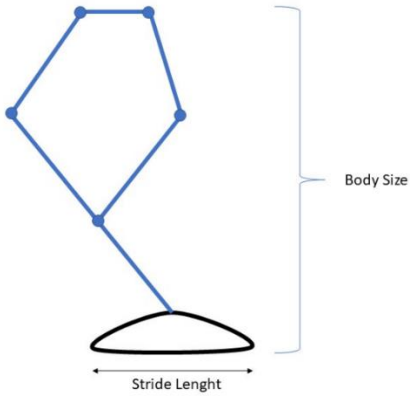

Figure 32: Stride length proportion to body size

6. Stride Straightness Ratio Percent: It shows that the mechanism draws a straight line in the walking path it creates, that is, the ratio of the step distance to the path fluctuating height. (Figure 33)

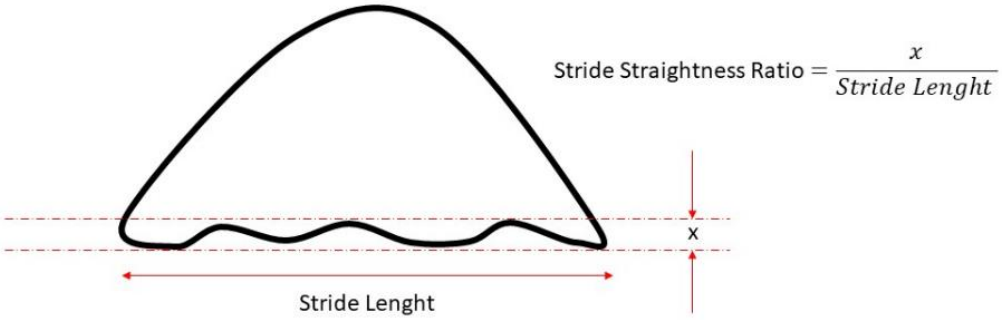

Figure 33: Stride straightness ratio percent

7. Velocity profile in the direction of stride: It shows the changes in the velocity perpendicular to the velocity of point P in the direction of the stride, i.e., during the stride. The smaller the change in velocity perpendicular to the direction of stride, the smoother the straight line formed by the mechanism.

8. Stride to footprint Ratio Percent: It expresses the ratio of the area covered by the mechanism to the distance the mechanism draws a straight line (Figure 34).

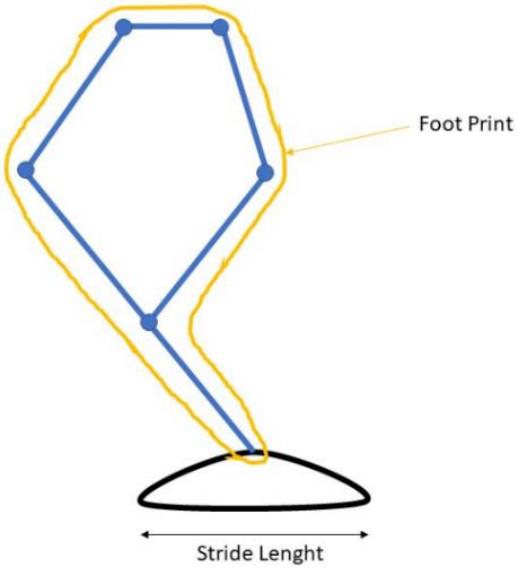

Figure 34: Stride to footprint ratio

Table 6: Comparison of walking mechanisms

#	Criteria	Jansen Linkage	Klann Linkage	Ghassaei Linkage	Desai Linkage	Fourbar -Pantog. Linkage	Proposed Over-constrained Linkage
1	**Number of links**	8,00	6,00	7,00	8,00	8,00	8,00
2	**Number of joints**	9,00	7,00	8,00	9,00	10,00	9,00
3	**Number of supports on the frame**	2,00	3,00	2,00	3,00	3,00	2,00
4	**Scalable**	No	No	No	No	No	Yes
5	**Stride length proportion to body size**	small	large	small	small	small	small-medium
6	**Stride straightness %**	3,90	4,20	1,45	3,70	1,10	1,50
7	**Velocity profile in the direction of stride**	fluctuating	fluctuating	straight	fluctuating	straight	fluctuating
8	**Stride to footprint ratio percent %**	0,29	0,16	0,25	0,22	0,30	0,15

In Figure 35, six different mechanisms are shown with acquired foot trajectory. The height of the compared mechanisms were chosen to be the same. Link lengths related to Jansen's mechanism are obtained from Ghassaei [2], and Klann's linkage is created with parameters from the work of Klann [30]. Ghassaei linkage is derived from the study of Ghassaei et al. [2]. Desai linkage is created according to link lengths given in the work of Desai et al. [12]. Parameters of the Four-bar-pantograph are taken from Ottaviano et al. [6].

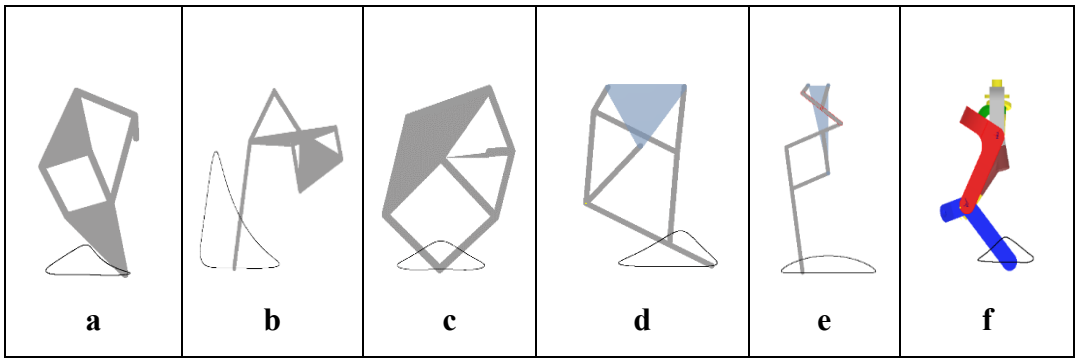

Figure 35: a) Jansen mechanism, b) Klann mechanism, c) Ghassaei mechanism, d) Desai mechansim, e) Fourbar Pantograph mechanism, f) Proposed overconstrained mechanism

The major difference between the proposed mechanism is the scalability of the trajectory by changing only the size of links 1, 2 and 3 as shown in Figure 36.

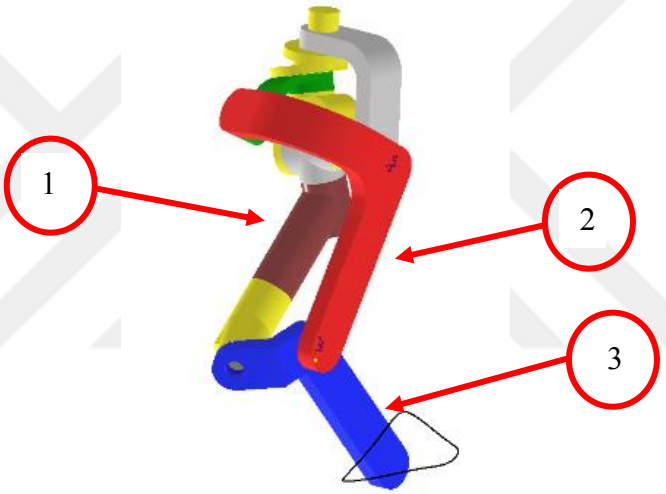

Figure 36: Links for scalability

Due to this property, the stride length proportion to body size can be variable by the scale of the mechanism for the desired motion. Also, being overconstrained, the proposed mechanism's stride to footprint ratio percent is small wrt other walking mechanisms. Lift is essential for walking mechanisms, whereas the lift in the mechanisms a-d can be described as medium proportional to its body size. The lift in the four-bar pantograph mechanism is negligible. In the proposed overconstrained mechanism, scalability helps determine the lift according to the purpose.

The accuracy of the data obtained from the dynamic simulation confirmed the comparisons made without the need to construct other mechanisms. When the torque values of the six mechanisms in Figure 37 are analyzed, it is seen that although it

oscillates slightly more than the other mechanisms, it has the lowest average torque value when it draws a straight line. In the case of installing a motor to meet the maximum torque value for the operation of the mechanism, the overconstrained walking mechanism will have less difficulty than the other mechanisms in the part where we assume that it draws a straight line.

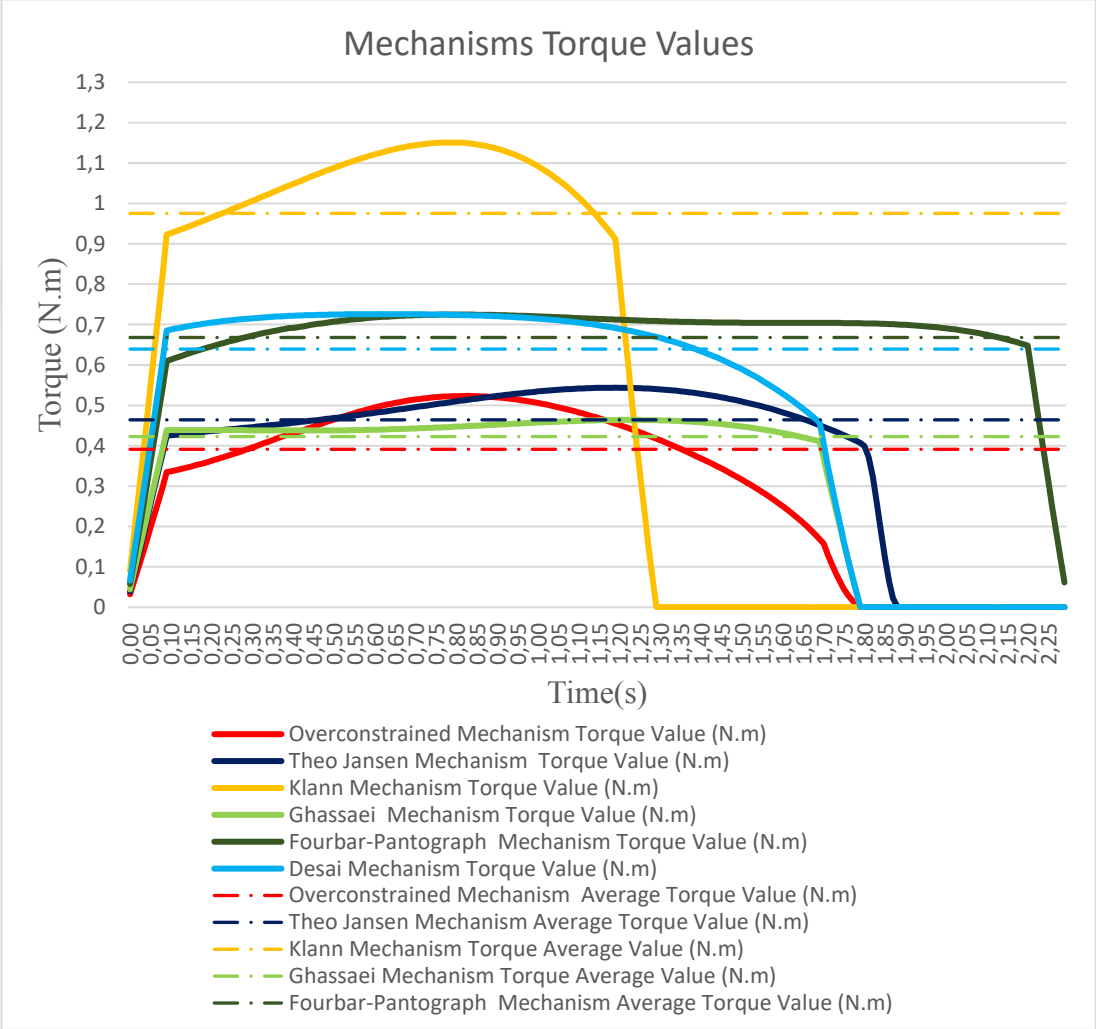

Figure 37: Torque values comparison for each mechanism

CHAPTER VI

CONCLUSION

In this thesis study, obtaining a walking mechanism from the overconstraint mechanism was aimed. During the thesis phase, dynamic simulation, kinematic analysis, and experimental tests were performed. At the end of all these studies, the advantages and disadvantages of the designed mechanism were extracted.

To check the correctness of the position equations obtained from the kinematic analysis, the walking paths obtained from the kinematic analysis were compared with the walking paths obtained from the dynamic simulation. The compared paths showed a very high degree of similarity. This provided the accuracy of the mechanism to a great extent. A test setup was prepared to see how these data would perform in real life. The test setup was created with the aim of giving the closest result to the analysis. However, some unexpected situations occurred during the tests. Some deviations and some irregularities were observed in the data. The reasons for these situations were objectively analyzed and explained. All errors that could be corrected were solved. Walking path and speed graphs were extracted from the test setup. The fact that these data obtained from the test setup matched the other datas mostly showed that this mechanism was successful. As a result of the analysis, simulation, and experiment, it was proved that overconstrained mechanisms can be used in walking mechanisms. This has opened the door to a new walking mechanism for those working in the areas of engineering or education.

In terms of scalability, which is a characteristic property of the mechanism, different walking paths were derived by changing only three of the eight links. Compared to other mechanisms in this field, the proposed overconstrained mechanism is much better. To prove this, four different scales of the mechanism were designed in the dynamic simulation stage and the walking paths of all of them were demonstrated. It was clearly seen that this mechanism would be more efficient to be used in limited areas, in situations where large or small walking paths need to be obtained.

For future work, the scalability of the mechanism can be utilized to obtain different walking paths by changing the lengths of the specified links during walking. In addition, the existing test setup could be improved, and more sensitive manufacturing and measurement tools could be used to correlate the analysis data with the test data. After these improvements, this mechanism will be preferred over others.

REFERENCES

[1] JANSEN Theo (2007), *The Great Pretender*, Ed. Illustrated, pp. 45-64, 010 Publishers, Rotterdam.

[2] GHASSAEI Amanda, CHOI Phil, and WHITAKER Dwight (2011), "The Design and Optimization of a Crank-Based Leg Mechanism", *Pomona College Department of Physics and Astronomy,* https://amandaghassaei.com/files/thesis.pdf, DoA. 07.06.2023.

[3] SUN-WOOK Kim, and DONG-HUN Kim (2011), "Design of Leg Length for a Legged Walking Robot Based on Theo Jansen Using PSO", *Journal of Korean Institute of Intelligent Systems*, Vol. 21, No. 5, pp. 660–666.

[4] ELARA Rajesh Mohan, NANSAI Shunsuke and IWASE Masami (2013), "Dynamic Analysis and Modeling of Jansen Mechanism", *Procedia Engineering*, Vol. 64, pp. 1562-1571.

[5] HYUN-GYU Kim, JUNG Min-Suck, SHIN Jae-Kyun, and SEO Tae Won (2014), "Optimal Design of Klann-Linkage Based Walking Mechanism for Amphibious Locomotion on Water and Ground", *Journal of Institute of Control,* Vol. 20, No. 9, pp. 936–941.

[6] OTTAVIANO Erika, GRANDE Salvatore, and CECCARELLI Marco (2010), "A Biped Walking Mechanism for a Rickshaw Robot", *Mechanics Based Design Of Structures and Machines*, Vol. 38, No. 2, pp. 227–242.

[7] DEB Kalyanmov and TIWARI Santosh (2005), "Multi-objective optimization of a leg mechanism using genetic algorithms", *Engineering Optimization*, Vol. 37, No. 4, pp. 325–350.

[8] SELVİ Özgün and YAVUZ Samet (2017), "Design and Dimensional Optimization of a Novel Walking Mechanism with Firefly Algorithm", *Mechanism and Machine Science*, Vol. 52, pp. 67-75.

[9] SELVİ Özgün, CECCARELLI Marco, and YAVUZ Samet (2019), "Design and optimization of a Walking Over-Constrained Mechanism", *Mechanisms and Machine Science*, Vol. 73, pp. 681–687.

[10] GEONEA Ionut Daniel, CĂTĂLIN Alexandru, MARGINE Alexandru, and UNGUREANU Alin (2013), "Design and Simulation of a Single DOF Human-Like Leg Mechanism", *Applied Mechanics and Materials*, Vol. 332, pp. 491–496.

[11] AL-ARAIDAH Omar, BATAYNEH Wafa DARABSEH, and TAHA Tariq (2011), "Conceptual design of a single DOF human-like eight-bar leg mechanism", *Jordan Journal of Mechanical and Industrial Engineering*, Vol. 5, No. 4, pp. 285-289.

[12] DESAI Shivamanappa, ANNIGERI Anandkumar, and GOUDA Timmana (2019), "Analysis of a new single degree-of-freedom eight link leg mechanism for walking machine", *Mechanism and Machine Theo.*, Vol. 140, pp. 747–764.

[13] FEDOROV Dimitri, BIRGLEN Lionel (2017), "Design of a Self-Adaptive Robotic leg using a triggered compliant element", *IEEE Robotics and Automation Letters*, Vol. 2, No. 3, pp. 1444–1451.

[14] WU Jianxu, YAO Yan-an (2018), "Design and analysis of a novel walking vehicle based on leg mechanism with variable topologies", *Mechanism and Machine Theory*, Vol. 128, pp. 663–681.

[15] SHIEH William, TSAI Lily, and AZARM Shapur (1997), "Design and optimization of a one-degree-of-freedom six-bar leg mechanism for a walking machine", *Journal of Field Robotics,* Vol. 12, No. 12, pp. 871-880.

[16] KAMIDI Vinay, SAAB Wael and BEN-TZVI Pinhas (2017), "Design and analysis of a novel planar robotic leg for high-speed locomotion", *IEEE/RSJ International Conference on Intelligent Robots and Systems (IROS),* pp. 6343-6348, Vancouver, Canada.

[17] GONG Yifeng, BEHR Alexander, GRAF Nicole, CHEN Kaiyi, and GONG Zhili (2022), "A walking claw for tethered object retrieval", *Journal of Mechanisms and Robotics*, Vol. 15, No. 5, DOI: 10.1115/1.4055812.

[18] KYLE James, YIM Justin, HART Kendall, BERGBREITTER Sarah, AARON Johnson (2023), "The Simplest Walking Robot: A bipedal robot with one actuator and two rigid bodies", *Arxiv Preprint*, DOI: 10.48550/arxiv.2308.08401.

[19] BHAVSAR Keval, GOHEL Dharmik, DARJI Pranav, MODI Jitendra, and PARMAR Umang (2020), “Kinematic analysis of Theo Jansen Mechanism-Based Eight-Leg Robot”, *In, Advances in Fluid Mechanics and Solid Mechanics Proceedings of the 63rd Congress of ISTAM 2018,* Ed. Domador Maity, Pradeep G. Siddheshwar, Sunanda Saha, pp. 75–82*,* Springer, Singapore, DOI: 10.1007/978-981-15-0772-4_6.

[20] LI Zhaolu, SONG Yumin, ZHANG Xiaoli, PENG Xiafu and Xu, Ning (2023), “Modeling of Walking-Gait parameters and walking strategy for quadruped robots”, *Applied Sciences*, Vol. 13, No. 12, DOI: 10.3390/app13126876.

[21] WANG Zhou, GE Wenjie, ZHANG Yonghong, LIU Bo, LIU Bin, JIN Shikai, and LI Yuzhu (2023), “Optimization design and performance analysis of a bionic knee joint based on the geared Five-Bar mechanism”, *Bioengineering*, Vol. 10, No. 5, DOI: 10.3390/bioengineering10050582.

[22] ANTONIO Gonzalez Rodriguez, ANGEL Gonzalez and PIERLUIGI Rea (2011), "A new articulated leg for mobile robots", *Industrial Robot*, Vol. 38, No. 5, pp. 521-532.

[23] GIESBRECHT Daniel, WU Christine, and SEPEHRI Nariman (2012), “Design And Optimization Of An Eight-Bar Legged Walking Mechanism Imitating A Kinetic Sculpture, “Wind Beast””, *Transactions of the Canadian Society for Mechanical Engineering*, Vol. 36, No. 4, pp. 343-355.

[24] BÖTTCHER Stefan (2006), “Principles of robot locomotion”, www2.cs.siu.edu/~hexmoor/classes/CS404-S09/RobotLocomotion.pdf, DoA. 23.06.2023.

[25] ZHONGHUA Shen and YINGMIAO Chen (2020), “Kinematics Analysis of a Quadruped Robot with Eight linkages Mechanism Based on Bar Group”, *In, Proceedings of the 2020 2nd International Conference on Big Data and Artificial Intelligence*, Ed. Rita Yi Man Li, Otillia Manta, Rebecca Kechen Dong, Ubaldo Comite, M. James C. Crabbe, pp.486–491, Association for Computing Machinery, New York, USA, DOI: 10.1145/3436286.3436442.

[26] GUTARRA Anthony, PALOMINO Styven, and ALEGRIA Elvis (2020), "Hexapod walking mechanism based on the Klann linkage for a 2 DOF amphibious robot", *In, Multibody Mechatronic Systems MuSME 2021 Papers from the MusMe Conference in 2020*, Volume 94, Ed. Martin Pucheta, Alberto Cardona, Sergio Preidikman, Rogelio Hecker, pp. 302–310, Springer, DOI: 10.1007/978-3-030-60372-4_34.

[27] NAIF Khalaf Al-Shammari (2020), "Dynamic simulation and design of a simple hexapod robot", *Indian Journal of Science and Technology*, Vol. 13, No. 36, pp. 3801–3819.

[28] YUPING Gu, SHIHAO Feng, YUQIN Guo, FANG Wan, JIAN Dai, JIA Pan and CHAOYANG Song (2022), "Overconstrained coaxial design of robotic legs with omni-directional locomotion", *Mechanism and Machine Theory*, Vol. 176, pp.105018, DOI: 10.1016/j.mechmachtheory.2022.105018.

[29] BATAYNEH Wafa, AL-ARAIDAH Omar, and MALKAWI Salahaddin (2013), "Biomimetic design of a single DOF Stephenson III leg mechanism", *Mechanical Engineering Research*, Vol. 3, No. 2, pp. 43-50.

[30] KLANN Joseph (2002), "Walking device (No. US6478314B1)", *US Patent and Trademark Office.*

[31] RUIQIN Hao, GUO Cheng, HAN Zeguang, and HAN Yu (2023), "Design and Research of Single Leg Walking Mechanism of Quadruped Robot", *Vibroengineering PROCEDIA*, Vol. 49, pp. 130–35.

[32] KONG Xianwen (2015), "Kinematic analysis of a 6R single-loop overconstrained spatial mechanism for circular translation", *Mechanism and Machine Theory*, Vol. 93, pp. 163–174.

[33] MING Lu, JING Baorui, DUAN Hao, and GAO Guanbin (2022), "Design of a Small Quadruped Robot with Parallel Legs", *Complexity*, Vol. 2022, pp. 1–11.

[34] LU Wenjuan, ZENG Jiahao, DONG Shihao, FAN Dabao, LIU Ya, ZENG Daxing, and CAO Miaoyan (2022), "Configuration design and gait analysis of Wheel-Legged mobile robot based on the Rubik's Cube mechanism", *IEEE Access*, Vol. 10, pp. 84473–84485.

[35] SAHA Subir, PRASAD Rajendra, and MANDAL Ananta (2003), "Use of Hoeken's and Pantograph Mechanisms for Carpet Scrapping Operations", *Proc. Of 11th Nat. Conf. On Machines and Mechanisms*, pp. 732-738, New Delhi.

[36] YINGMIAO Chen (2019), “Design of a New Type of Eight-bar Walking Mechanism based on Regeneration Kinematic Chain Method and Artas SAM”, *International Journal for Research in Applied Science and Engineering Technology*, Vol. 7, No. 12, pp. 674–682.

[37] ALİZADE Rasim, BAYRAM Cağdaş, and GEZGİN Erkin (2007), “Structural synthesis of serial platform manipulators”, *Mechanism and Machine* Theory, Vol. 42, No. 5, pp. 580-599.

[38] SELVİ Özgün (2012), *Structural and kinematic synhthesis of overconstrained mechanisms* (Doctoral Dissertation), Izmir Institute of Technology, İzmir.

[39] SHOJAEI Amir Mohammad (2023), *Interfacing DRV8825 Stepper Motor Driver Module with Arduino*, https://electropeak.com/learn/interfacing-drv8825-stepper-motor-driver-module-with-arduino/, DoA. 25.07.2023.

APPENDICES

APPENDIX 1: MATLAB CODE

```
const int dirPin = 3;
const int stepPin = 4;
bool motorRunning = false; // Flag to indicate if the motor is currently running
bool clockwiseDirection = true; // Flag to indicate the current direction of rotation, true
for clockwise
void setup() {
pinMode(stepPin, OUTPUT);
pinMode(dirPin, OUTPUT);
Serial.begin(9600);
}
void loop() {
if (motorRunning) {
// Set the direction based on the clockwiseDirection flag
digitalWrite(dirPin, clockwiseDirection ? HIGH: LOW);

// Step the motor once (no acceleration)
digitalWrite(stepPin, HIGH);
delay(6);
digitalWrite(stepPin, LOW);
delay(6);
}
}
void executeCommand(char command) {
 // Perform actions based on the received command
switch (command) {
case 'X':
```

```
motorRunning = false; // Stop the motor
Serial.println("Motor stopped.");
break;
case 'C':
motorRunning = true; // Start the motor
clockwiseDirection = true; // Set clockwise rotation
Serial.println("Motor started with clockwise rotation.");
break;
case 'U':
motorRunning = true; // Start the motor
clockwiseDirection = false; // Set counterclockwise rotation
Serial.println("Motor started with counterclockwise rotation.");
break;
default:
Serial.println("Invalid command. Use X, C, or U.");
break;
}
}
void serialEvent() {
while (Serial.available()) {
char command = Serial.read();
executeCommand(command);
}
}
```

APPENDIX 2: TOP PLATE TECHNICAL DRAWING

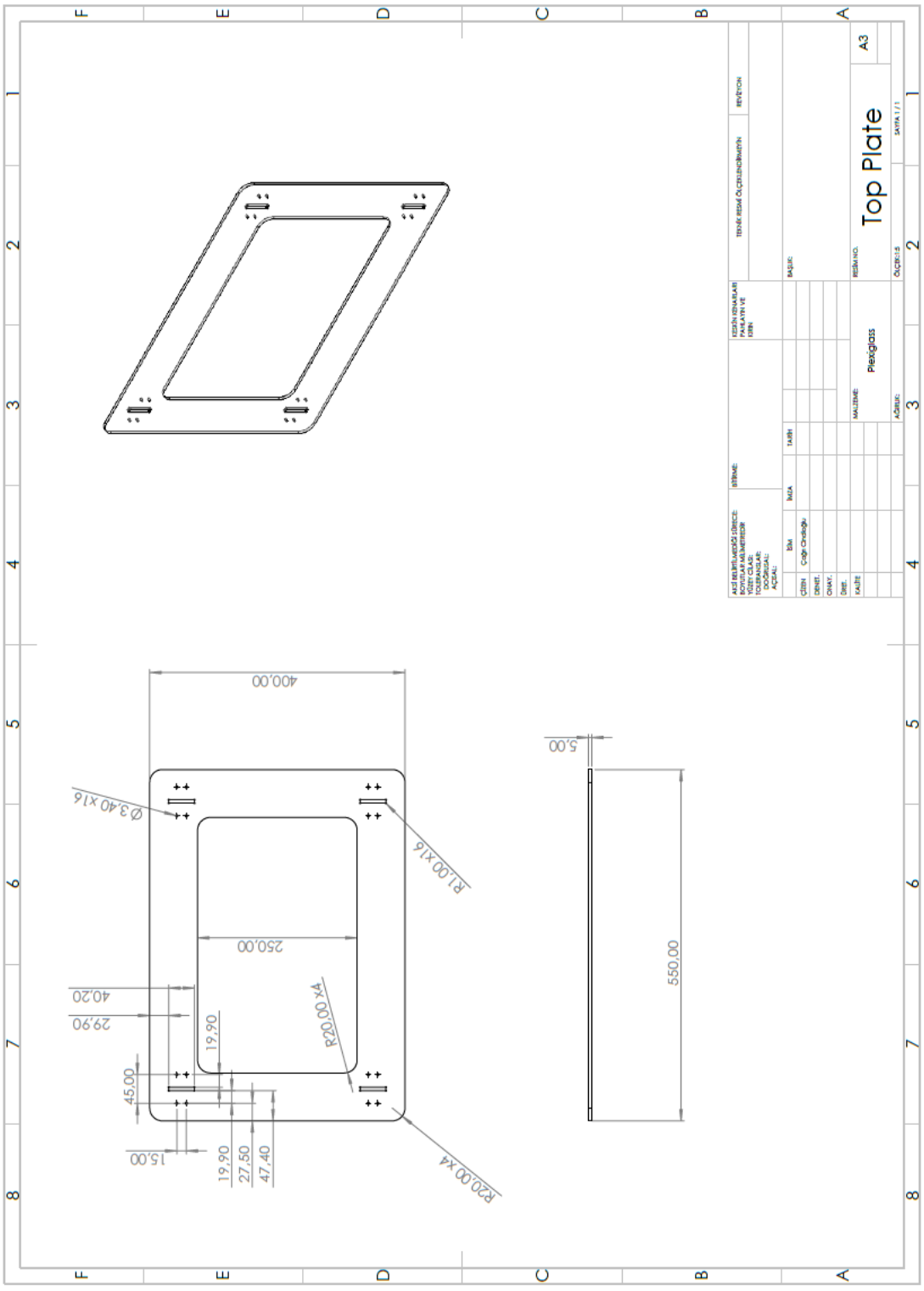

APPENDIX 3: BOTTOM PLATE TECHNICAL DRAWING

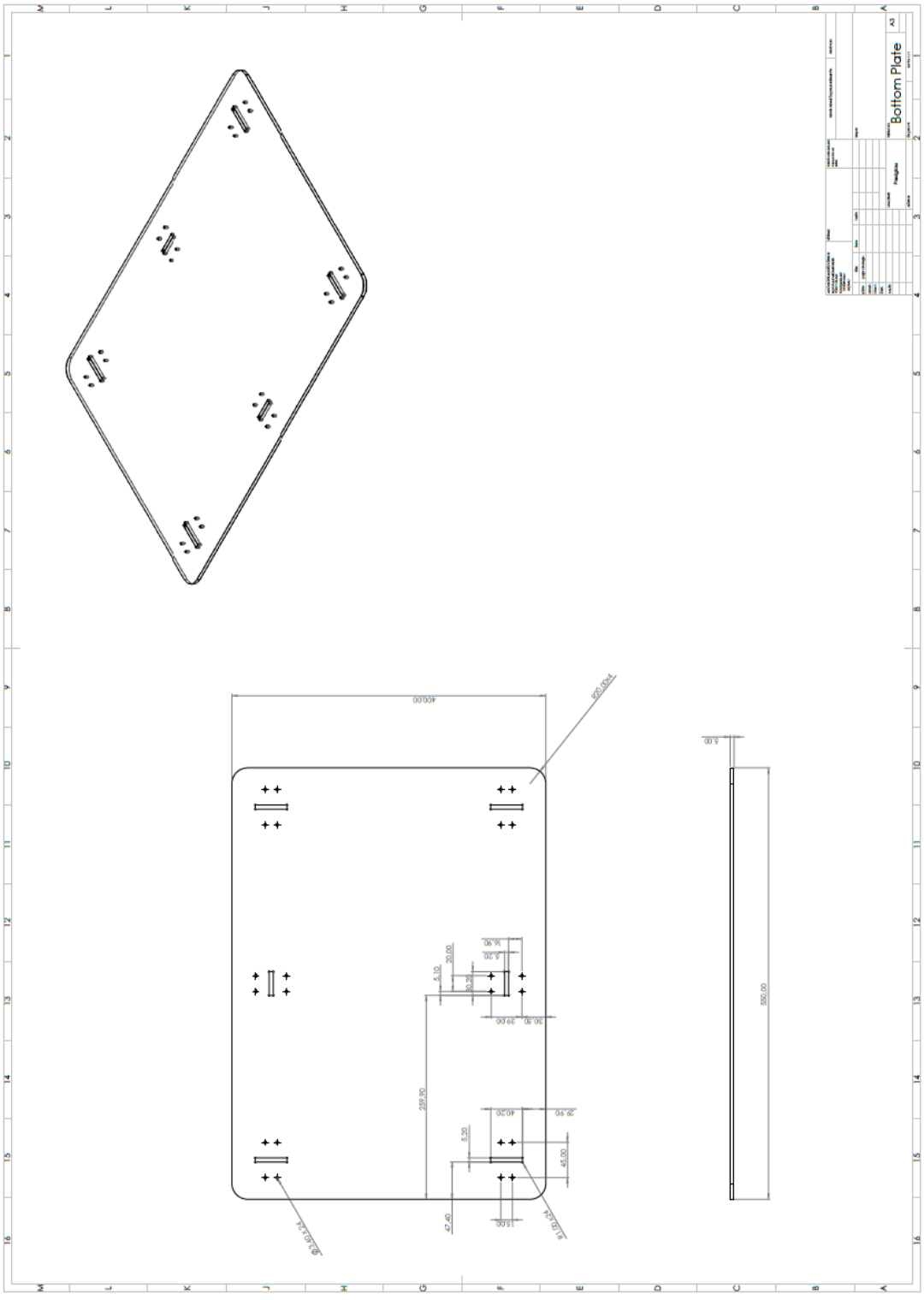

APPENDIX 4: MOVABLE PLATE TECHNICAL DRAWING

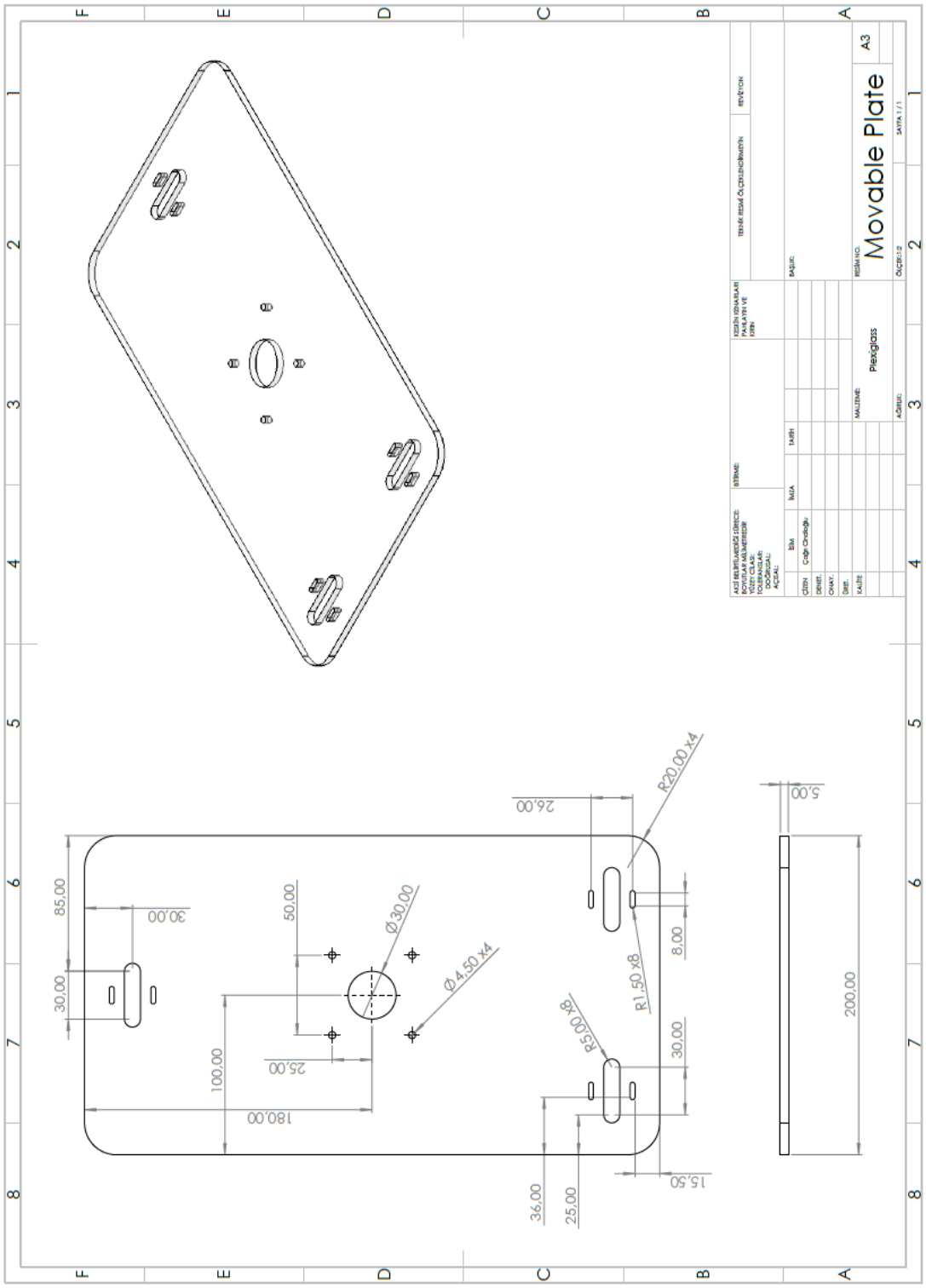

APPENDIX 5: V SUPPORT TECHNICAL DRAWING

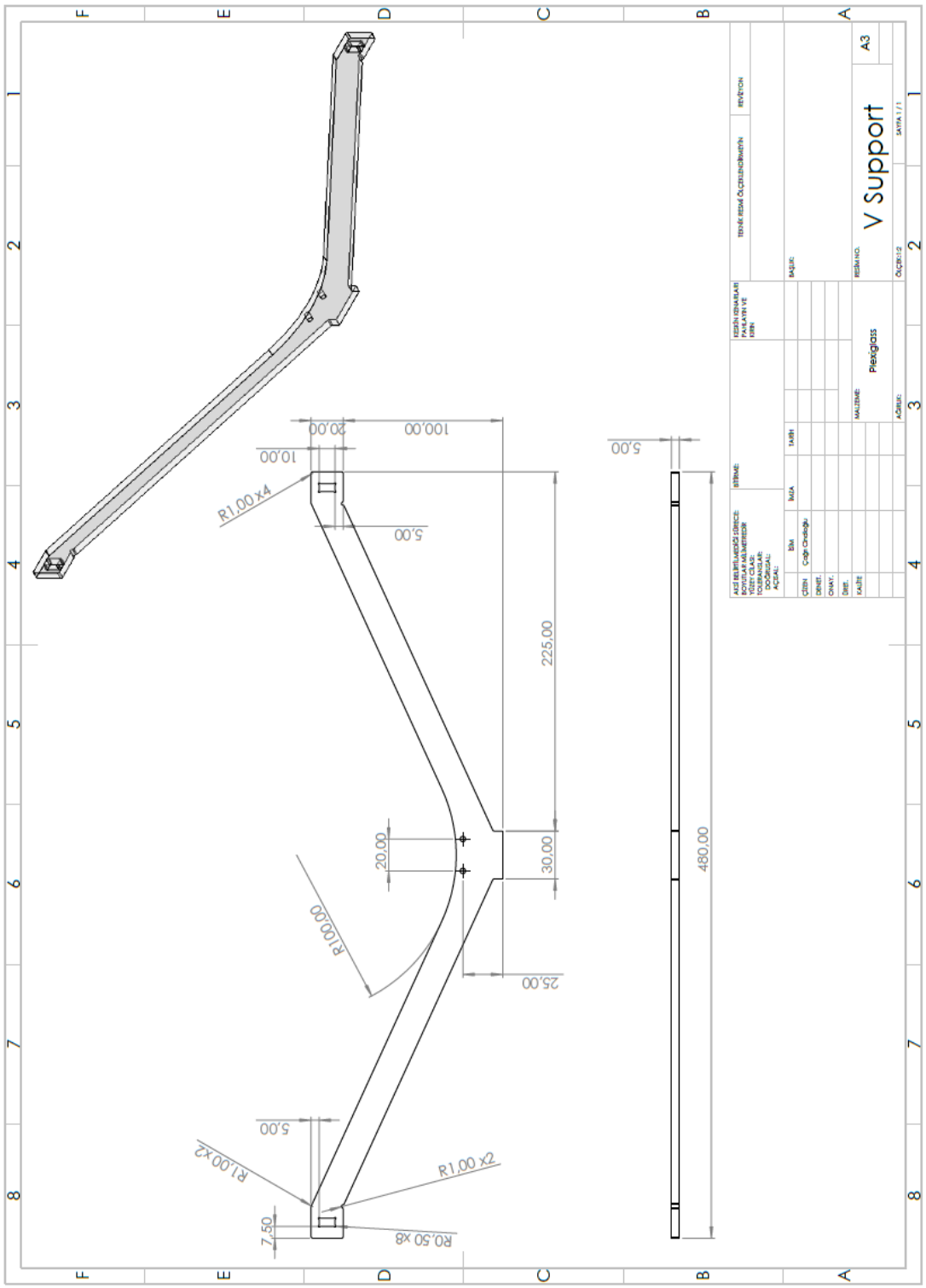

APPENDIX 6: COLUMN TECHNICAL DRAWING

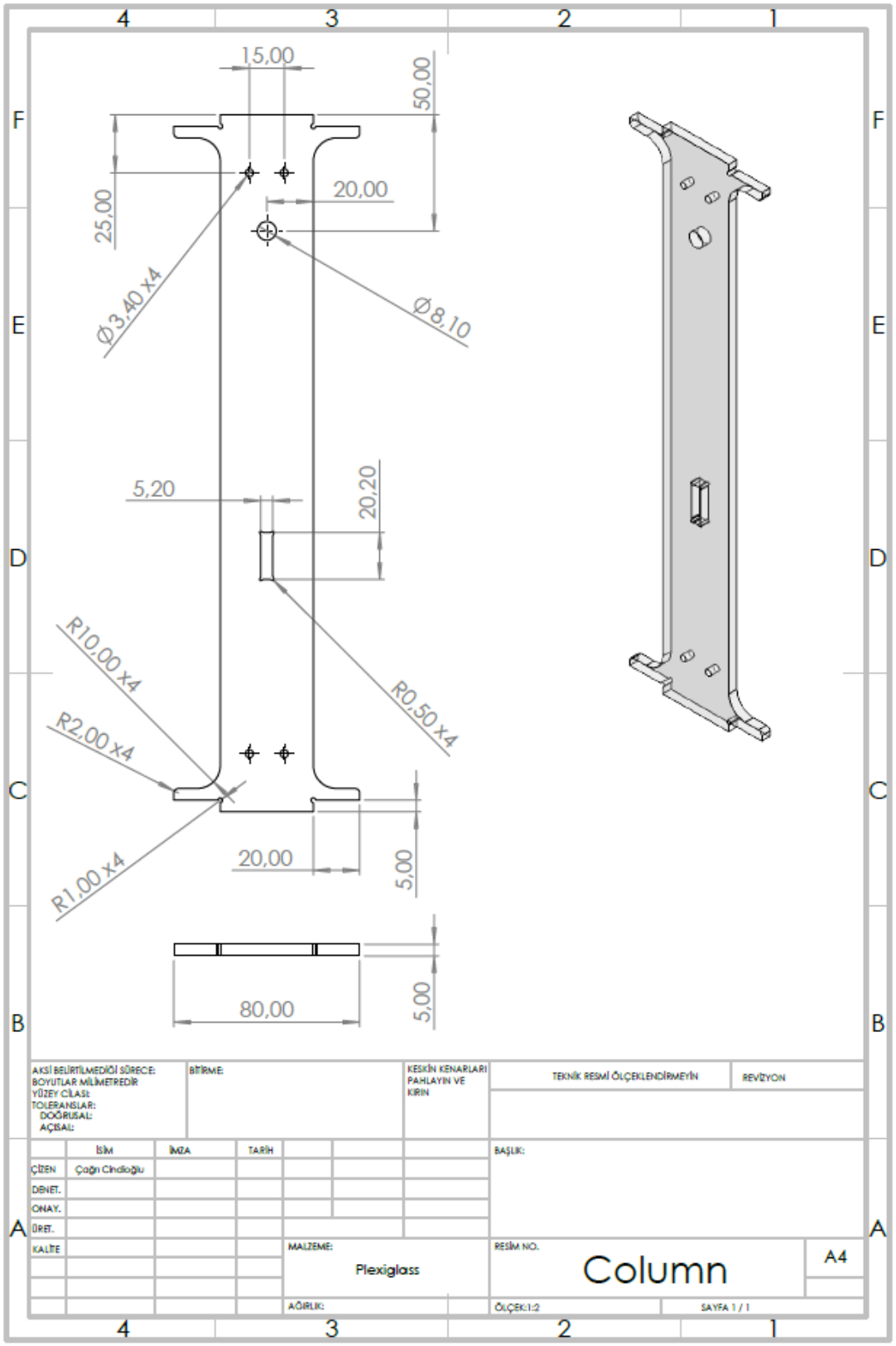

APPENDIX 7: TOP SIDE MOTOR HOLDER TECHNICAL DRAWING

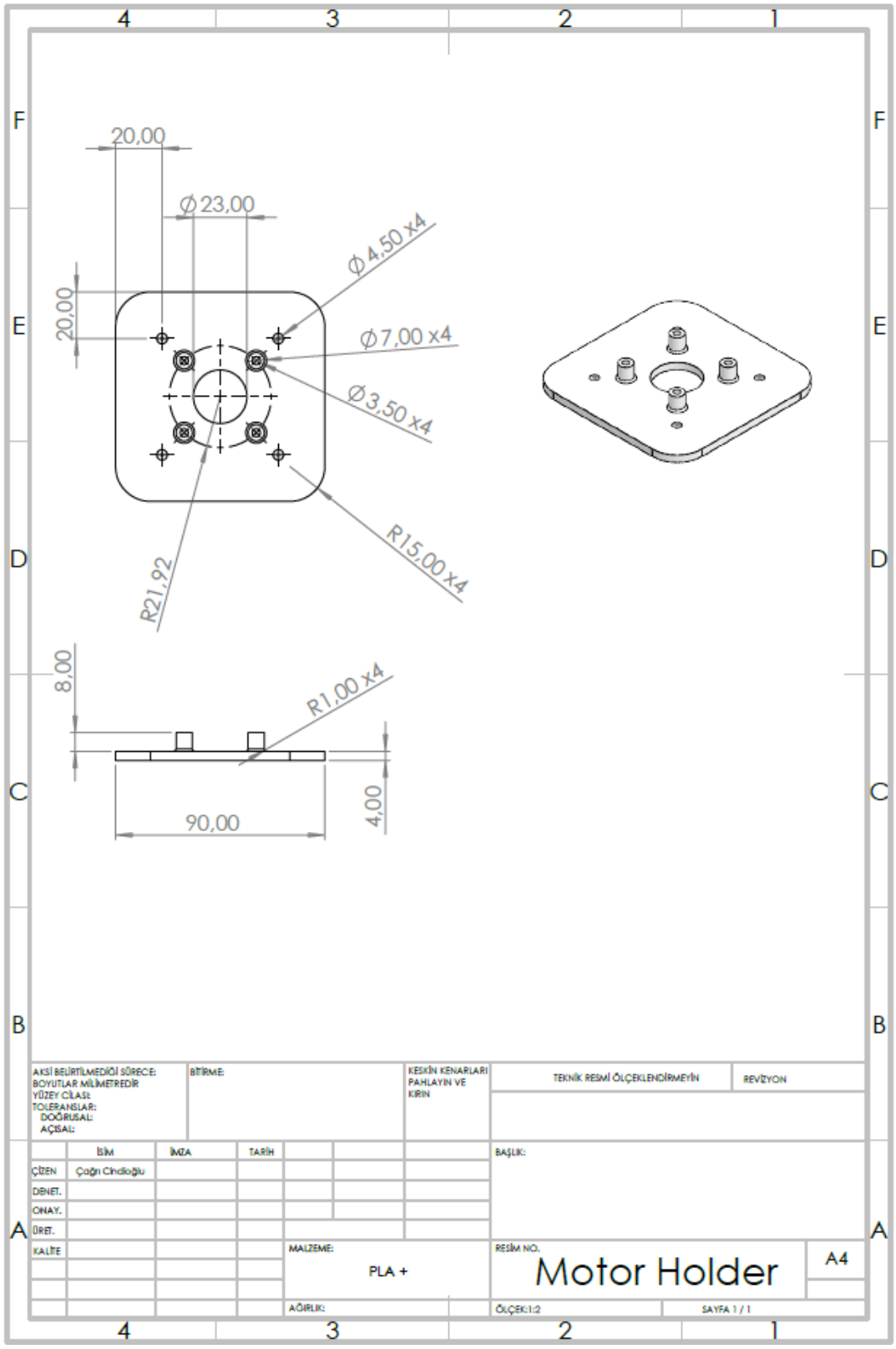

APPENDIX 8: BOTTOM SIDE MOTOR HOLDER TECHNICAL DRAWING

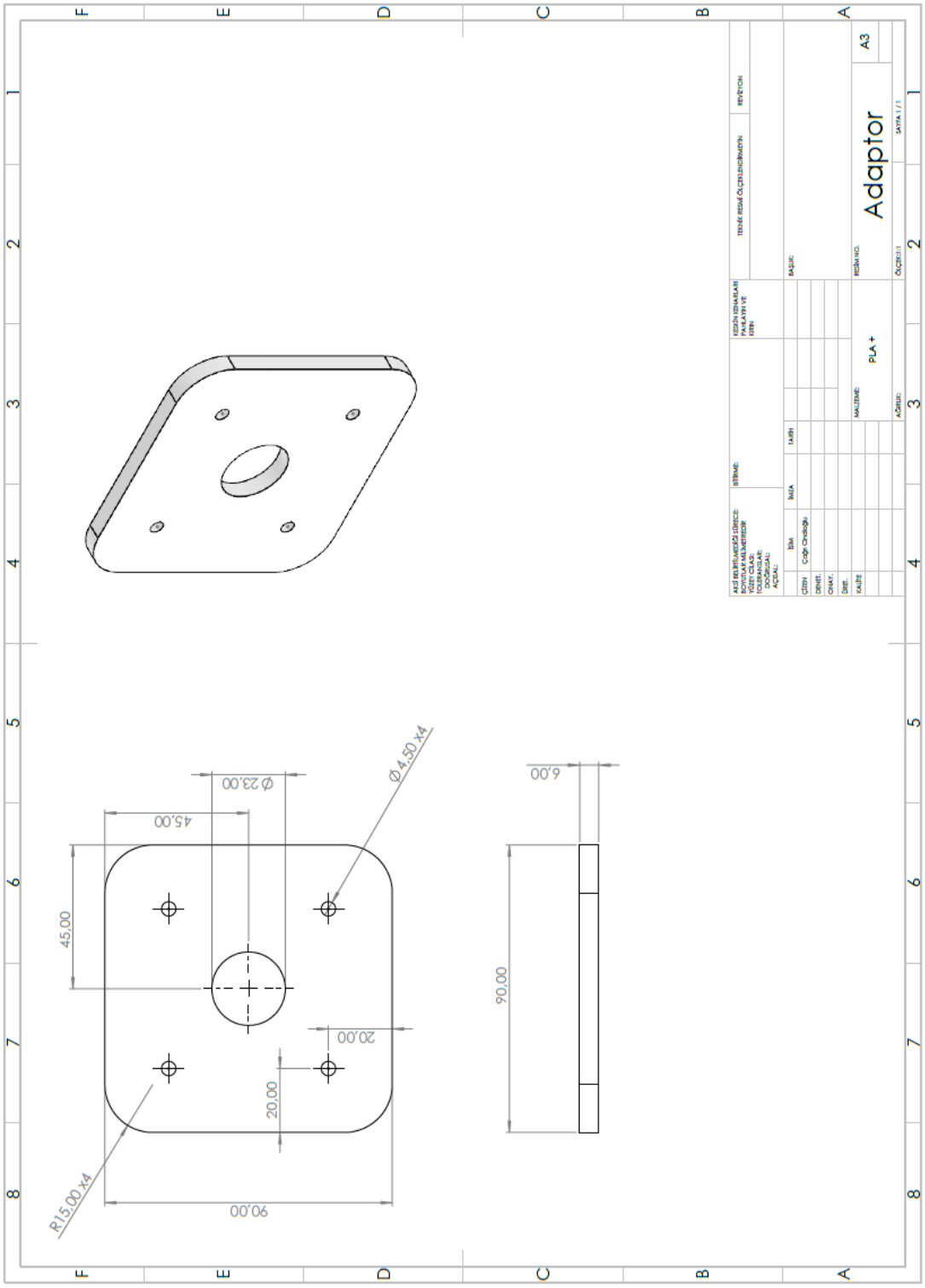

APPENDIX 9: L BRACKET FOR V PART TECHNICAL DRAWING

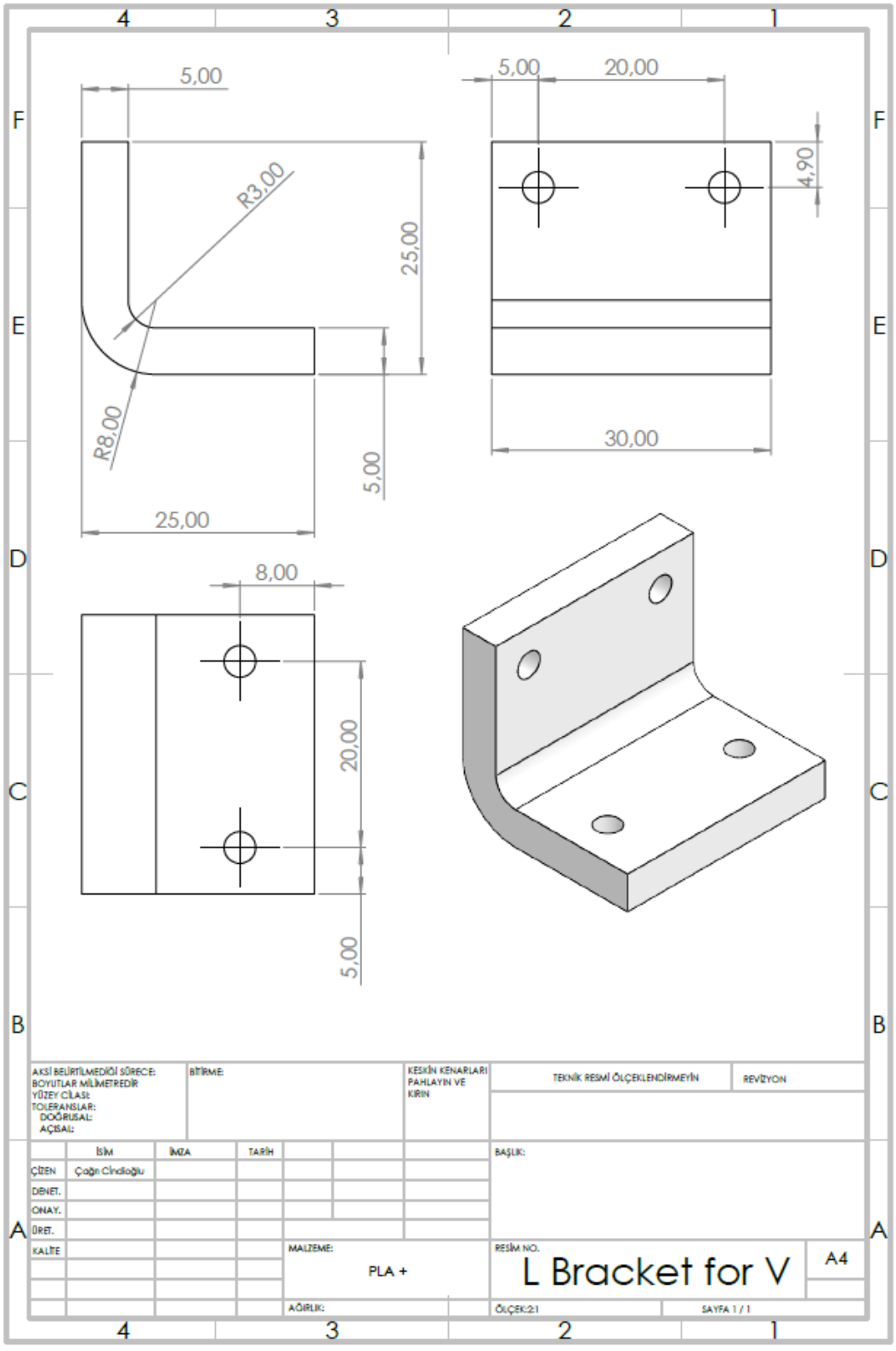

APPENDIX 10: L BRACKET TECHNICAL DRAWING